A conserved cell division protein directly regulates FtsZ dynamics in filamentous and unicellular actinobacteria

Felix Ramos-Léon[1†], Matthew J. Bush[1†], Joseph W. Sallmen[1], Govind Chandra[1], Jake Richardson[2], Kim C. Findlay[2], Joseph R. McCormick[3], Susan Schlimpert[1*]

Affiliations

1 Department of Molecular Microbiology, John Innes Centre, Norwich, UK
2 Department of Cell and Developmental Biology, John Innes Centre, Norwich, UK
3 Department of Biological Sciences, Duquesne University, Pittsburgh, USA

† These authors contributed equally to this work

* Correspondence: susan.schlimpert@jic.ac.uk

Keywords:

Streptomyces, mycobacteria, FtsZ, sporulation, development, cell division

Abstract

Bacterial cell division is driven by the polymerization of the GTPase FtsZ into a contractile structure, the so-called Z-ring. This essential process involves proteins that modulate FtsZ dynamics and hence the overall Z-ring architecture. Actinobacteria, like *Streptomyces* and *Mycobacterium* lack known key FtsZ-regulators. Here we report the identification of SepH, a conserved actinobacterial protein that directly regulates FtsZ dynamics. We show that SepH is crucially involved in cell division in *Streptomyces* and that it binds FtsZ via a conserved helix-turn-helix motif, stimulating the assembly of FtsZ protofilaments. Comparative *in vitro* studies using the SepH homolog from *Mycobacterium* further reveal that SepH can also bundle FtsZ protofilaments, indicating an additional Z-ring stabilizing function *in vivo*. We propose that SepH plays a crucial role at the onset of cytokinesis in actinobacteria by promoting the rapid assembly of FtsZ filaments into division-competent Z-rings that can go on to mediate septum synthesis.

Introduction

Cell division is an essential process for almost all living organisms. The core component of the bacterial cell division machinery is the bacterial tubulin homolog FtsZ, which forms the so-called Z-ring at the future division site. Like tubulin, FtsZ monomers polymerize in a GTP-dependent manner into cytoplasmic filaments that undergo treadmilling *in vivo,* a process in which FtsZ subunits are selectively added to one end and removed from the other end (Loose and Mitchison, 2014; Yang et al., 2017). The Z-ring provides a dynamic scaffold for the assembly of a multiprotein division machinery, the divisome. In addition, FtsZ treadmilling also guides the circumferential movement of peptidoglycan synthases at the division site which leads to septum formation and cell membrane constriction (Bisson-Filho et al., 2017; Perez et al., 2019; Yang et al., 2017).

While the rate of treadmilling is set by the FtsZ GTPase activity, the overall architecture of the Z-ring is modulated by FtsZ-binding proteins that can influence its positioning, membrane interaction or stimulate FtsZ filament formation and bundling (Caldas et al., 2019; García-Soriano et al., 2020; McQuillen and Xiao, 2020). The function of many of these proteins has been well-characterized in the classical rod-shaped model organisms *E. coli* and *B. subtilis*. However, members of the actinobacteria, which include industrially and medically important species such as the prolific antibiotic producers of the genus *Streptomyces*, or the human pathogens *Mycobacterium tuberculosis* and *Corynebacterium diphtheriae*, lack most of the key components that are known to regulate the dynamics of Z-ring formation. This raises the fundamental question as to how exactly the assembly and the architecture of the Z-ring is controlled in these bacteria.

Streptomyces are Gram-positive soil bacteria that have a fascinating multicellular life cycle involving filamentous growth and sporulation (Bush et al., 2015). Unlike most unicellular organisms that assemble one Z-ring and divide by binary division, *Streptomyces* have two functionally distinct modes of cell division: vegetative cross-wall formation and sporulation septation (Figure 1A). Cross-walls divide the growing mycelium occasionally into long multigenomic compartments that remain physically connected. In contrast, during reproductive growth, dozens of sporulation septa are simultaneously deposited in a ladder-like pattern between the segregating chromosomes along the length of sporogenic hyphae. Sporulation septa eventually constrict, leading to cell-cell separation and the release of unigenomic spores. Both these forms of cell division require FtsZ, but unlike in most other bacteria the *ftsZ* gene can be deleted in *Streptomyces,* leading to viable hyphae that lack both cross-walls and sporulation septa (McCormick et al., 1994; Santos-Beneit et al., 2017). The *Streptomyces* divisome is comprised of several conserved core divisome components including FtsQ, DivIC, FtsL, FtsEX, and the cell wall synthesis proteins FtsI and FtsW (McCormick, 2009). In addition,

the *Streptomyces* cell division machinery includes the membrane anchor SepF, two additional SepF-like proteins of unknown function (SepF2 and SepF3), the two dynamin-like proteins DynA and DynB, which ensure the stability of Z-rings during sporulation and the actinomycete-specific protein SsgB, which has been proposed to recruit FtsZ to future sporulation septation sites (Schlimpert et al., 2017; Willemse et al., 2011). However, factors that affect the dynamics of Z-ring formation and regulate its architecture have not yet been identified in actinobacteria and the mechanisms that control cell division in *Streptomyces* and related actinobacteria are poorly understood.

Here, we report the identification and characterization of SepH, a conserved actinobacterial-specific cell division protein that directly binds FtsZ and regulates the dynamics of Z-ring formation in filamentous *Streptomyces* and in rod-shaped *Mycobacterium* species. We find that SepH co-localizes with FtsZ in *Streptomyces* and is required for regular cross-wall formation and sporulation septation. Biochemical characterization of SepH from *Streptomyces venezuelae* and *Mycobacterium smegmatis* revealed that SepH interacts with FtsZ via a highly conserved helix-turn-helix motif and stimulates the rapid formation of FtsZ protofilaments *in vitro*. In addition, SepH from *M. smegmatis* promotes the lateral interaction of FtsZ filaments. Our data suggest that SepH fulfils a crucial function in the initial stages of cell division by increasing the local concentration of FtsZ, thereby stimulating the assembly of division-competent Z-rings.

Results

SepH is required for regular sporulation in *Streptomyces venezuelae*

In *Streptomyces*, the initiation of sporulation-specific cell division is controlled by two key transcriptional regulators, WhiA and WhiB. Recent work by Bush et al. determined the regulon of WhiA and WhiB, which co-control the expression of ~240 transcriptional units (Bush et al., 2016, 2013). To identify novel regulators of Z-ring formation in actinomycetes, we chose to focus on uncharacterized gene products which are conserved across streptomycete genomes and are direct targets of WhiAB (Figure 1-figure supplement 1). This analysis turned our attention to *vnz_27360* (here named *sepH for "septation protein H"*), a gene of previously unknown biological function that is conserved across the *Streptomyces* genus. Bioinformatic analysis revealed that SepH consists of an N-terminal domain of unknown function (DUF3071) and an unstructured, less conserved C-terminal half (Figure 1B). In addition, the DUF3071 domain contains a predicted helix-turn-helix motif (HTH) suggesting that SepH could function as a DNA-binding protein.

To investigate if *sepH* plays a role in *Streptomyces* cell division, we first generated a Δ*vnz_27360::apr* null mutant (Δ*sepH*) and imaged sporulating hyphae of wild-type *S. venezuelae* (WT), Δ*sepH* and the complemented Δ*sepH* mutant strain (Δ*sepH*/*sepH*$^+$) by cryo-scanning electron microscopy (cryo-SEM) (Figure 1C). While aerial hyphae of wild-type *S. venezuelae* completely differentiate into chains of regularly sized spores, *sepH*-deficient hyphae failed to undergo efficient sporulation septation, leading to chains of spores of irregular size (Figure 1-figure supplement 2). This phenotype could be fully complemented by providing *sepH in trans* (Δ*sepH/sepH*$^+$), suggesting that SepH is indeed required for normal sporulation.

Next, we set out to determine the subcellular localization of SepH and generated a C-terminal SepH-YPet fusion. The *sepH-ypet* fusion, controlled by its native promoter, was integrated *in trans* at the ΦBT1 phage attachment site in a strain that was engineered to additionally produce mCherry labelled FtsZ, allowing us to visualize the sites of cell division. Microscopic analysis of the resulting *S. venezuelae* strain revealed that SepH-YPet co-localized specifically with FtsZ-mCherry at incipient division sites including vegetative cross-walls and sporulation septa (Figure 1D). Although *sepH* is a direct target of the two sporulation-specific regulators WhiAB, the accumulation of SepH-YPet at vegetative division septa suggests that *sepH* expression is probably driven from an additional, WhiAB-independent promoter and that SepH might also be involved in cell division during vegetative growth.

Furthermore, we asked whether the specific localization pattern of SepH is dependent on FtsZ and the assembly of a functional divisome. To address this question, we took advantage of an Δ*ftsZ* null mutant (Santos-Beneit et al., 2017) and inserted a *sepH-ypet* fusion

in trans. Fluorescence microscopy of the Δ*ftsZ* strain constitutively producing SepH-YPet revealed that in the absence of FtsZ, SepH-YPet is largely stable and dispersed in the cytoplasm but occasionally accumulates in random foci (Figure 1-figure supplement 3A and B), indicating that SepH recruitment to future division sites depends upon the assembly of Z-rings.

SepH is important for cell division during vegetative growth and sporulation

To determine the role of SepH in *Streptomyces* cell division, we introduced a fluorescent *ftsZ-ypet* fusion into the Δ*sepH* mutant strain and wild-type *S. venezuelae* and followed the formation of Z-rings during sporulation using time-lapse fluorescence microscopy. In sporulating wild-type hyphae, Z-rings are assembled in a characteristic, "ladder-like" pattern in the tip cell compartment of sporogenic hyphae. These so-called "Z-ladders" lead to the synthesis of sporulation septa and the formation of chains of exospores of equal size (Figure 2A and Supplementary Movie 1). Interestingly, in the Δ*sepH* mutant Z-ladders were less uniform and frequently displayed an irregular spacing between individual FtsZ-YPet-rings. As observed in cryo-SEM images, spores produced under these conditions were aberrant in size and shape, indicating that regular septation was impaired (Figure 2B and Supplementary Movie 2).

Kymograph analyses of FtsZ-YPet fluorescence in sporulating wild-type hyphae confirmed the expected regular spacing and dynamics of Z-rings, including Z-ring assembly and constriction, which is accompanied with an increase in fluorescence followed by disassembly and loss of defined FtsZ-YPet fluorescence. In contrast, establishment of equally spaced Z-rings frequently failed in SepH-deficient hyphae leading to the formation of larger, spore-like compartments (Figure 2C and D and Figure 2-figure supplement 1A and B). Notably, closer inspection of the gaps within Z-ladders in Δ*sepH* hyphae revealed that no FtsZ-YPet signal was visible at these positions, indicating that the formation of individual Z-rings was disturbed very early in the assembly process. We note that FtsZ protein levels are similar in sporulating WT and Δ*sepH* cultures (Figure 2-figure supplement 2), indicating that the absence of SepH does not affect FtsZ protein stability. Furthermore, Z-ring assembly is not completely impaired in every sporogenic Δ*sepH* hypha, suggesting that additional mechanisms might be in place that can partially compensate for the lack of SepH activity.

While analyzing the spatiotemporal localization of FtsZ-YPet in Δ*sepH* hyphae, we noticed occasional lysis of large hyphal segments and the formation of unusual branched sporogenic hyphae (Figure 2B). Given that FtsZ and SepH also co-localize at cross-walls (Figure 1D), we reasoned that the absence of SepH might also affect cell division during vegetative growth. To examine the importance of SepH for cross-wall formation, we used the

fluorescent D-ala-D-ala analogue HADA, to label peptidoglycan and to visualize cross-walls (Kuru et al., 2015). Inspection of still images of wild-type *S. venezuelae* (WT) and the complemented Δ*sepH* mutant strain (Δ*sepH/sepH*$^{+}$) grown in the presence of HADA showed comparable frequency and distribution of cross-walls within vegetative hyphae. However, we found that *sepH*-deficient hyphae displayed visibly fewer cross-walls compared to WT (Figure 2E). The dramatically reduced number of cross-walls in the *sepH* mutant could explain the lysis and branching phenotype we observed in our Δ*sepH* time-lapse microscopy experiments. In wild-type *Streptomyces*, cross-walls compartmentalize growing hyphae and are often associated with hyphal branch points leading to the physical separation of different hyphal segments. Thus, fewer cross-walls in the Δ*sepH* mutant result in much longer hyphal compartments that are potentially more susceptible to large-scale lytic events. In addition, at the onset of sporulation septation, FtsZ ladders assemble within these unsegmented and branching hyphal compartments which can subsequently result in the formation of the enlarged triangular shaped-like spores at hyphal branch points (Figure. 2B). Collectively, these results demonstrate a crucial role for SepH in cell division during vegetative growth and sporulation.

The N-terminal DUF3071 domain is crucial for SepH function.

To identify the protein regions required for the recruitment and function of SepH, we generated fluorescent protein fusions to the N-terminal DUF3071 domain (SepH-NTD, residues 1-186) and the unstructured C-terminal domain (SepH-CTD, residues 187-344) (Figure 3A). The corresponding mutant alleles were integrated *in trans* at the ΦBT1 attachment site in the Δ*sepH* null mutant and expressed from the native promoter. The resulting strains were then analyzed by fluorescence microscopy and cryo-SEM to determine the subcellular localization of the fusion proteins and their ability to compensate for the loss of wild-type SepH activity. Using automated Western blotting, we verified that all proteins were synthesized and stable under the conditions used (Figure 3-figure supplement 1). Control experiments with full-length SepH-YPet demonstrated that this fusion was fully functional and restored wildtype-like localization and sporulation (compare Figure 3B, F and Figure 3-figure supplement 2). Expression of the SepH C-terminal domain (SepH-CTD) gave a diffuse localization pattern and failed to complement any aspect of the Δ*sepH* phenotype, resulting in irregular sporulation and cell lysis (Figure 3C and G). Interestingly, in contrast, production of the N-terminal DUF3071 domain (SepH-NTD) was sufficient to partially restore normal sporulation (Figure 3H). However, the distinct septal accumulation characteristic of full-length SepH-YPet and wildtype-like sporulation could only be clearly observed for the truncated gene fusion when it was constitutively expressed in the Δ*sepH* mutant (Figure 3E and I). Taken together, these

results imply that the conserved N-terminal region of SepH encoding the DUF3071 domain is vital for SepH function, but wild-type activity also requires the C-terminal domain.

SepH does not bind to the nucleoid

The DUF3071 domain of SepH includes a helix-turn-helix (HTH) motif, characteristic of DNA binding proteins (Aravind et al., 2005). This raised the question as to whether SepH could interact with the nucleoid. Notably, to-date, no functional homologs of the well-described nucleoid occlusion systems present in other bacteria have been identified in *Streptomyces*. To investigate a potential role of SepH in chromosome segregation, we first generated a dual-labelled strain which produced SepH-YPet and an mCherry-labelled version of the bacterial nucleoid-associated protein HupA (Salerno et al., 2009). Both fluorescent protein gene fusions were integrated at the ΦBT1 attachment site of wild-type *S. venezuelae* and expression was driven from their native promoters. Fluorescence microscopy of the resulting *S. venezuelae* strain showed that SepH-YPet and HupA-mCherry did not co-localize. Instead, SepH-YPet accumulated at sites where HupA-mCherry was largely absent, indicating that SepH does not associate with the nucleoid (Figure 4A). Furthermore, we visualized the nucleoid in wild-type and Δ*sepH* spore chains stained with the fluorescent DNA dye 7-AAD but did not observe anucleate spores in the Δ*sepH* mutant (Figure 4B), suggesting that chromosome segregation is not impaired in *sepH*-deficient hyphae.

To independently verify our localization studies, we first performed chromatin immunoprecipitation coupled to deep-sequencing (ChIP-seq) using sporulating wild-type *S. venezuelae*. In parallel, we conducted ChIP-seq with the Δ*sepH* mutant strain as a negative control to eliminate false-positive signals arising from non-specific binding of the α-SepH antibody. Analysis of the ChIP-seq results did not reveal any significant enrichment of SepH on the chromosome (Figure 4-figure supplement 1A) compared to the Δ*sepH* negative control. Furthermore, DNase I footprinting experiments using purified SepH together with radiolabeled probes derived from three of the most enriched chromosomal regions (Figure 4-figure supplement 1B), did not reveal protection of the selected DNA fragments, collectively suggesting that SepH does not bind to specific DNA-sequences. Finally, we performed electrophoretic mobility shift assays (EMSAs) to test SepH for non-specific DNA-binding activity *in vitro* (Figure 4-figure supplement 1C). For this, we tested binding of SepH to the promoter region of *vnz_35870* (the most enriched region from ChIP-seq), the sequence internal to *vnz_08520* (not enriched in ChIP-seq) and the low GC-sequence of the kanamycin resistance gene from a standard *E. coli* expression vector. Under the conditions used, we did not observe binding of SepH to any of these DNA fragments. Collectively, our results strongly

suggest that the HTH motif in the conserved N-terminal region of SepH is not involved in DNA binding and that SepH does not play a direct role in chromosome segregation.

The SepH helix-turn-helix motif is essential for the interaction with FtsZ

While most HTH motifs mediate DNA binding, exceptions to this rule exist and HTH motifs have also been shown to facilitate protein-protein interaction (van den Ent et al., 2010). Thus, we hypothesized that the HTH motif within the NTD of SepH could directly affect the function of a protein binding partner, such as FtsZ or other components of the *Streptomyces* cell division machinery. To investigate this possibility, we performed yeast-two hybrid (Y2H) assays. As previously described, we observed that FtsZ can self-interact and associate with SepF (Schlimpert et al., 2017). Furthermore, our Y2H experiments suggest that SepH can oligomerize and, most significantly, SepH binds FtsZ (Figure 5A). In addition, we tested interactions between SepH and several other *Streptomyces* divisome components including SepF, SepF2, SepF3, DynA and DynB but only detected a putative interaction with SepF in one orientation (Figure 5-figure supplement 1).

To identify the SepH domain involved in binding FtsZ, we performed additional experiments using the SepH-NTD and the SepH-CTD variants (Figure 5B). We found that the SepH-NTD could bind FtsZ in the Y2H assays but the SepH-CTD could not. We hypothesized that the HTH fold in the N-terminal domain of SepH could be involved in binding FtsZ. Thus, we repeated the Y2H assay with a SepH variant in which we had substituted a highly conserved glycine residue in the HTH motif with a proline residue (SepH-G79P) (Mercy et al., 2019). While SepH-G79P was still able to interact with wild-type SepH (Figure 5B), this mutant version failed to bind FtsZ. This indicated that the SepH HTH motif is indeed required for the interaction with FtsZ, but not for self-interaction. We also introduced the *sepH*-G79P allele into the Δ*sepH* mutant and found that SepH-G79P was unable to restore wildtype-like sporulation (Figure 5-figure supplement 2).

Encouraged by the Y2H results, we purified recombinant *S. venezuelae* FtsZ, SepH and the SepH mutant variants to test if SepH can directly influence the behavior of FtsZ *in vitro* (Figure 5C). Using circular dichroism (CD), we confirmed that the G79P substitution did not cause any major structural changes (Figure 5-figure supplement 3A). We then examined SepH and its variants by size exclusion chromatography and found that wild-type SepH, SepH-CTD and SepH-G79P elute as one peak, corresponding to a predicted size of a tetramer, while SepH-NTD eluted as a dimer (Figure 5-figure supplement 3B). We next measured the GTP hydrolysis rate of FtsZ in the presence of SepH (Figure 5D). Initial characterization of the biochemical properties of *S. venezuelae* FtsZ confirmed that the protein was active and robustly hydrolyzed GTP in a time-dependent manner at a rate of 1.12 ± 0.44 GTP per FtsZ

per minute, similar to the recently published activity of *Streptomyces* FtsZ (Figure 5-figure supplement 3C) (Sen et al., 2019). While SepH on its own does not hydrolyze GTP, we found that the addition of increasing amounts of SepH led to a moderate increase of FtsZ's GTP turnover (Figure 5D). Importantly, we observed a similar stimulation of the GTPase activity when we incubated FtsZ with SepH-NTD variant but not with SepH-CTD or SepH-G79P.

To further substantiate our finding that SepH directly binds FtsZ, we performed high-speed sedimentation assays (Figure 5F). In the absence of GTP, FtsZ was unable to polymerize into filaments and was largely found in the supernatant after ultracentrifugation. In the presence of GTP, approximately 18% of FtsZ was detected in the pellet fraction, indicating that FtsZ had assembled into polymers. When SepH was added to the reaction with FtsZ and GTP prior to ultracentrifugation, more than 54% of FtsZ and 61% of SepH were co-sedimented, confirming a direct interaction between SepH and FtsZ. In contrast, incubation of FtsZ with GTP and the SepH variant carrying the mutant helix-turn-helix motif (SepH-G79P) resulted in a clearly reduced co-sedimentation of SepH-G79P (28%) with polymerized FtsZ (39%). In addition, in the absence of FtsZ both SepH and SepH-G79P were largely soluble.

The enrichment of SepH and FtsZ in the pellet fraction following high-speed centrifugation suggested that SepH either promotes the formation of macromolecular FtsZ bundles or stimulates the assembly of a high number of individual FtsZ protofilaments. To further distinguish between these two possibilities, we repeated this co-sedimentation assay at a lower centrifugation speed that would only allow the pelleting of FtsZ bundles. A similar approach was recently employed to examine the assembly state of FtsZ filaments in complex with the FtsZ-stabilizing protein GpsB (Eswara et al., 2018). Using this differential centrifugation method, we found that low-speed centrifugation did not lead to an accumulation of SepH and FtsZ in the pellet fraction (Figure 5-figure supplement 4). Taken together, our two-hybrid and *in vitro* experiments demonstrate that SepH directly interacts with FtsZ via the HTH motif in the conserved N-terminal DUF3071 domain. Furthermore, this interaction appears to stimulate the abundant formation of FtsZ protofilaments, rather than bundles, which would account for the observed increase in GTPase activity of FtsZ.

SepH stimulates the rapid formation of dynamic FtsZ filaments *in vitro*

To further investigate the assembly state of FtsZ and to visualize the effect of SepH on FtsZ filament morphology, we used negative staining and transmission electron microscopy (TEM). Our control experiments confirmed that purified FtsZ and SepH did not form any visible complexes when imaged on their own (Figure 6A and B). When the polymerization buffer (50 mM HEPES pH 7.2, 50 mM KCl, 5 mM $MgCl_2$) contained 3.5 μM FtsZ and 2 mM GTP, FtsZ

formed long, gently curved fibers that sparsely covered the EM grid (Figure 6C). In contrast, in the presence of GTP and 3.5 μM SepH, FtsZ filaments were readily visible as largely straight filaments of various lengths (Figure 6D). Closer inspection of these FtsZ filaments revealed that the addition of SepH did not increase filament width compared to FtsZ polymers formed in the absence of SepH (Figure 6E). This supports our co-sedimentation data, suggesting that SepH stimulates the efficient assembly of FtsZ protofilaments but does not seem to promote lateral interactions between filaments. These results are also consistent with an increase in FtsZ GTPase activity as a direct consequence of the high abundance of FtsZ protofilament ends that can undergo treadmilling.

In addition, we examined FtsZ filament assembly in the presence of the different SepH mutant variants. As expected, incubation of FtsZ with GTP and SepH-CTD or SepH-G79P did not alter FtsZ filament morphology (Figure 6-figure supplement 1A and B). However, adding SepH-NTD to FtsZ and GTP resulted in filaments similar in appearance to FtsZ filaments formed with full-length SepH (Figure 6-figure supplement 1C), corroborating our earlier findings that the SepH DUF3071 domain with the HTH motif drives the interaction with FtsZ.

To directly follow the assembly kinetics of purified FtsZ into filaments, we used dynamic light scattering (DLS). In the presence of 50 μM GTP, FtsZ monomers assembled into protofilaments which resulted in a sharp increase in the light scattering signal. The reaction reached a brief steady-state level before GTP became limiting and the intrinsic FtsZ GTPase activity triggered depolymerization and the complete disassembly of FtsZ filaments. In contrast, incubation of 3.5 μM FtsZ with 50 μM GTP and increasing amounts of SepH led to a significantly higher amplitude in light scattering compared to FtsZ with just GTP (Figure 6F). This was followed by a rapid decrease in light scattering and the complete depolymerization of FtsZ filaments. As expected, control experiments using GDP or SepH with GTP did not generate a meaningful light scattering signal (Figure 6-figure supplement 2A). Furthermore, we recorded the polymerization dynamics of FtsZ in combination with the different SepH mutant variants. In agreement with our earlier results, SepH-NTD stimulated FtsZ assembly dynamics in a similar manner to wild-type SepH (Figure 6-figure supplement 2B). However, we noticed that FtsZ filaments formed under these conditions appeared to be more stable, suggesting that the C-terminal domain of SepH has some influence on the overall activity of SepH and the interaction with FtsZ. As anticipated, SepH-CTD and SepH-G79P did not further promote the assembly of FtsZ filaments and resulted in scatter profiles similar to FtsZ alone with GTP.

We repeated the DLS experiments using a higher GTP concentration (2mM) to test if the detected decrease in light scattering was caused by the depletion of GTP and the

accumulation of GDP. When GTP is provided in excess, there is no drop in the light scatter signal (Figure 6-figure supplement 2C), suggesting that the observed decline in the scatter signal in Figure 7F was in fact caused by the depolymerization of FtsZ filaments.

In addition, we monitored FtsZ polymerization in the presence of SepH and the slow-hydrolysable GTP analogue GMPCCP to test if GTP hydrolysis is required for SepH-stimulated FtsZ filament assembly. We observed a clear increase in the light scattering signal compared to reactions without SepH (Figure 6G), indicating that SepH-induced FtsZ protofilament formation does not depend on GTP hydrolysis. This result was further supported by TEM images of FtsZ filaments assembled in the presence of GMPCCP and SepH. Incubation with FtsZ and GMPCCP led to the formation of long and stable FtsZ polymers (Figure 6-figure supplement 3A). Addition of SepH resulted in a visible increase of these long and curved FtsZ polymers that occasionally further associated into straight multifilament bundles, which was likely an indirect effect due to increased longitudinal filament stability (Figure 6-figure supplement 3B). Together, these findings demonstrate that SepH directly regulates the behavior of FtsZ by promoting the rapid and reversible assembly of FtsZ protofilaments.

SepH is conserved in morphologically diverse actinobacteria

Previous work by Gao et al. (Gao et al., 2006) identified a group of 24 so-called signature proteins that are highly conserved actinobacterial proteins and SepH was one of these 24 proteins. To get a better understanding of the phylogenetic distribution and conservation of SepH, we specifically searched for SepH homologs in an expanded set of 3962 representative genomes, including those of 673 actinobacterial species.

In total, we identified 626 SepH homologs, which, in agreement with Gao et al., are exclusively found in actinobacteria (Figure 7A) (Gao et al., 2006). Furthermore, SepH homologs cluster into distinct groups, suggesting a greater sequence divergence at the family level. Interestingly, in contrast to SepH homologs detected in e.g. the Coreynbacteriales or Micrococcales, SepH homologs identified in all analyzed streptomycetes genomes (n=60) display a very high sequence identity (>80%), which is reflected by the small number of individual leaves within the Streptomycetales branch. Notably, members of the actinobacteria display remarkably diverse cellular morphologies, ranging from cocci and rods to multicellular filaments (Barka et al., 2016). Thus, it is conceivable that SepH homologs have further evolved to support cell division in the different actinobacterial species.

Despite this apparent divergence of SepH homologs throughout the actinobacteria, a refined alignment of 360 SepH sequences clearly showed a strong conservation in the N-terminal DUF3071 domain, including the helix-turn-motif (Figure 7-figure supplement 1).

Interestingly, we identified two additional sequence motifs that are highly conserved among SepH homologs. These include a lysine and arginine-rich patch, which is particularly enriched in SepH sequences from *Corynebacteria*, and ten amino acids at the far C-terminal end of SepH homologs (Figure 7-figure supplement 1). It is conceivable that these residues are involved in a yet unidentified aspect of SepH function.

To investigate if SepH homologs share a similar biological function, we expressed codon-optimized *sepH* from the non-pathogenic, rod-shaped model organism *Mycobacterium smegmatis* mc^2 155 (*sepH*$_{Ms}$, *MSEMG_5685*) in the *S. venezuelae* Δ*sepH* mutant. Both SepH homologs share an overall sequence identity of 34%. The heterologous *sepH*$_{Ms}$ was fused to *mcherry*, placed under the control of the native *sepH* promoter and integrated at the *S. venezuelae* ΦBT1 phage attachment site. SepH$_{Ms}$-mCherry was able to fully support wildtype-like sporulation in the Δ*sepH* mutant (Figure 7B). Moreover, SepH$_{Ms}$-mCherry also displayed the characteristic septal localization in growing and sporulating hyphae similar to SepH from *S. venezuelae* (Figure 1D and 7B). In addition, we could detect a direct interaction between SepH$_{Ms}$ and FtsZ$_{Ms}$ using yeast two-hybrid analyses, supporting the idea that SepH plays a universal role in actinobacterial cell division (Figure 8C).

SepH from mycobacteria stimulates FtsZ polymerization and bundling

To test if SepH$_{Ms}$ can also affect the behavior of FtsZ$_{Ms}$ *in vitro*, we purified recombinant SepH$_{Ms}$-6xHis (SepH$_{Ms}$) and untagged FtsZ$_{Ms}$ (Figure 7-figure supplement 2). We first examined SepH$_{Ms}$ by size exclusion chromatography and found that it eluted, like SepH from *S. venezuelae*, as a single peak that corresponds to the predicted size of a tetramer (148 kDa) (Figure 7-figure supplement 3). We also measured the effect of SepH$_{Ms}$ on the GTPase activity of FtsZ$_{Ms}$ but did not observe a significant effect on the GTP turnover rate when SepH$_{Ms}$ was added to the reaction (Figure 7-figure supplement 4). Next, we followed the assembly of FtsZ$_{Ms}$ into filaments using DLS. As described previously, mycobacterial FtsZ displays a significantly lower polymerization rate than FtsZ from *E. coli* (White et al., 2000). However, FtsZ$_{Ms}$ polymerization was dramatically stimulated upon addition of SepH$_{Ms}$ at a molar ratio of 1: 0.5 (Figure 7D), as indicated by a sharp and rapid increase in the light scattering signal. Electron microscopy of negatively stained FtsZ$_{Ms}$ (6 μM) confirmed that the incubation with GTP led to the assembly of long and thin protofilaments (Figure 7E). Interestingly, and in contrast to SepH from *S. venezuelae*, the addition of 3 μM SepH$_{Ms}$ resulted in the formation of FtsZ$_{Ms}$ bundles, which were even more prominent when FtsZ$_{Ms}$ and SepH$_{Ms}$ were combined at equimolar concentrations (Figure 7-figure supplement 5). Notably, in the background of these bundles, shorter FtsZ filaments were visible, suggesting that SepH$_{Ms}$ initially enhances FtsZ$_{Ms}$ protofilament formation which subsequently leads to the assembly of long and stable FtsZ$_{Ms}$

418 filaments that can further associate into stable multifilament bundles. We could further support
419 $SepH_{Ms}$-mediated $FtsZ_{Ms}$ bundling by differential co-sedimentation experiments. Incubation of
420 $FtsZ_{Ms}$ with GTP and $SepH_{MS}$ followed by either high- or low-speed centrifugation led to an
421 enrichment of both proteins in the pellet (Figure 7F), indicating that $SepH_{Ms}$ leads to the
422 formation of macromolecular FtsZ assemblies that can be pelleted at lower centrifugation
423 rates. This clearly suggests that $SepH_{Ms}$ not only stimulates the rapid polymerization of $FtsZ_{Ms}$
424 but also has the propensity to promote lateral interactions of $FtsZ_{Ms}$ filaments.
425 Collectively, our results demonstrate that SepH from mycobacteria accelerates and
426 stimulates the assembly of $FtsZ_{Ms}$ filaments, in a similar manner to SepH from *S. venezulae*.
427 In addition, $SepH_{Ms}$ further promotes lateral interactions between $FtsZ_{Ms}$ protofilaments,
428 leading to the formation of stable macromolecular FtsZ assemblies *in vitro*.
429
430

Discussion

Here we report the identification of SepH as one of the missing actinomycete-specific positive regulators of Z-ring formation. Based on our *in vivo* and *in vitro* characterization of the SepH homologs from the filamentous species *S. venezuelae* and the rod-shaped species *M. smegmatis*, we propose a model in which SepH-mediated FtsZ assembly increases the local concentration of FtsZ. This in turn promotes the spatial ordering of FtsZ filaments, the formation of division-competent Z-ring(s) and efficient FtsZ treadmilling, which is linked to the synthesis of septal peptidoglycan (Figure 8) (Bisson-Filho et al., 2017; Yang et al., 2017).

Our model is supported by several lines of evidence. First, we demonstrate that SepH plays a crucial role during the early stages of Z-ring formation. Kymograph analysis of fluorescently tagged FtsZ revealed that individual Z-rings fail to assemble in sporulating *S. venezuelae* hyphae lacking SepH (Figure 2C). Notably, this contrasts with earlier results from a *Streptomyces* Δ*dynAB* mutant in which already assembled Z-rings become destabilized and disassemble, leading to failed septation or partially constricted hyphae (Schlimpert et al., 2017). Thus, SepH is clearly important for the establishment of Z-rings. In addition, *Streptomyces* undergo a second, distinct mode of division during vegetative growth which leads to the synthesis of cross-walls. Our live-cell imaging studies revealed that SepH is not only required for sporulation-specific cell division but also for vegetative cross-wall formation (Figure 2E). The formation of cross-walls is poorly understood and although the synthesis of cross-walls depends on FtsZ, other core cell division proteins such as FtsI, FtsL and FtsW are not required (McCormick, 2009). We found that deleting *sepH* significantly reduced the number of cross-walls in vegetative hyphae. The importance of SepH for FtsZ-mediated cell division during vegetative growth was further supported by the observation that SepH-deficient hyphae were prone to extensive cell lysis due to the lack of hyphal compartmentalization. This is in line with work by Santos-Beneit et al. demonstrating that cross-walls protect the mycelium from large scale cell rupture caused by mechanical or enzymatical stress (Santos-Beneit et al., 2017). Thus, despite the different morphological outcomes of the two types of cell division that occur during the *Streptomyces* life cycle, both require SepH for efficient and regular Z-ring formation (Figure 8).

Second, we show that SepH directly interacts with FtsZ *in vitro* and determined the protein domain that are critical for SepH function. Our cytological and biochemical analyses have revealed that the N-terminal DUF3071 domain is crucial for SepH activity during cell division (Figure 3 and 5). Importantly, our data support the idea that SepH function depends on a highly conserved helix-turn-helix motif located within the DUF3071 domain (Figure 7-figure supplement 1). Mutational analysis confirmed that this motif is essential for SepH activity

in *S. venezuelae* cell division and required for interaction with FtsZ (Figure 5). Further structural studies will be required to identify the critical residues at the interface of the SepH-FtsZ complex and to determine whether SepH association induces a conformational change in the FtsZ structure that could promote the rapid nucleation and/or bundling observed in our *in vitro* experiments. Although the SepH C-terminus is less conserved among SepH homologs and largely dispensable for SepH function, we found that the C-terminal domain (CTD) is required for SepH tetramer formation *in vitro* and efficient subcellular localization *in vivo* (Fig. Figure 5-figure supplement 3B and Figure 3). In support of the importance of the C-terminal half for SepH function, we identified two additional short sequence motifs of unknown function within the CTD that are widely conserved among SepH homologs (Figure 7-figure supplement 1).

Third, we demonstrate that SepH from *S. venezuelae* and $SepH_{Ms}$ from *M. smegmatis* stimulate FtsZ nucleation and affect FtsZ filament stability which ultimately may aid the formation of division-competent Z-rings *in vivo* (Figure 6 and 7). Recent work in *B. subtilis* and *S. aureus* suggest that at the onset of cytokinesis, loose FtsZ filaments are actively condensed into a Z-ring. This process depends on FtsZ treadmilling and the activity of FtsZ-binding proteins, such as SepF, FtsA, ZapA or GpsB, which support filament formation, bundling, stabilization or membrane-anchoring (Eswara et al., 2018; Monteiro et al., 2018; Silber et al., 2020; Squyres et al., 2020; Whitley et al., 2020; Woldemeskel et al., 2017). Interestingly, our *in vitro* studies suggest that the SepH homologs from *S. venezuelae* and *M. smegmatis* display biochemical properties that are partially similar to the activities described for ZapA and GspB (Caldas et al., 2019; Eswara et al., 2018; Squyres et al., 2020; Woldemeskel et al., 2017). For example, similar to the effect described for GpsB, we found that SepH and $SepH_{Ms}$ stimulate FtsZ assembly (Eswara et al., 2018). In addition, like ZapA, *M. smegmatis* $SepH_{Ms}$ also supports lateral association of FtsZ filaments (Caldas et al., 2019). Our *in vitro* studies suggest slightly contrasting results for the effects of SepH and $SepH_{Ms}$ on the GTPase activity of FtsZ (Figure 5D and Figure 7-figure supplement 4). We believe that the observed 2-fold increase in the GTPase rate of FtsZ in the presence of *S. venezuelae* SepH is an indirect consequence of the more abundant and reversible assembly of FtsZ filaments (Figure 6F). However, the net effect of both SepH homologs leads to a local increase in FtsZ concentration which is likely to influence FtsZ GTPase activity, thereby mediating efficient FtsZ-treadmilling and Z-ring remodeling. Moreover, like GpsB and ZapA, both characterized SepH homologs form oligomers in solution which could further aid the assembly of FtsZ filaments into a condensed Z-ring to drive cytokinesis.

Finally, our combined cytological, biochemical and phylogenetic analyses support our hypothesis that SepH plays a conserved and crucial role in actinobacterial cell division. Actinobacteria display a range of complex lifestyles and include human pathogens such as

Corynebacterium diphtheriae or *Mycobacterium tuberculosis*, in which *sepH* is essential (Barka et al., 2016; Griffin et al., 2011; Sassetti et al., 2003). Although SepH is not essential in *S. venezuelae*, SepH-deficient hyphae are subject to frequent cell lysis during vegetative growth and sporulate less efficiently (Supplementary Movie 2), supporting the notion about the critical role of SepH in actinobacterial development.

In summary, we propose that SepH functions to stimulate FtsZ polymerization and in this way orchestrates the assembly, stabilization and activity of FtsZ at the onset of cell division in actinobacteria.

Materials and Methods

Bacterial strains and growth conditions

Bacterial strains are listed in Supplementary File 1 (Table 1). *E. coli* strains were grown in LB or LB agar at 37°C supplemented with the following antibiotics when necessary: 100 µg mL^{-1} carbenicillin, 50 µg mL^{-1} kanamycin, 25 µg mL^{-1} hygromycin, 50 µg mL^{-1} apramycin or 25 µg mL^{-1} chloramphenicol.

Streptomyces venezuelae was grown in maltose-yeast extract-malt extract medium (MYM) prepared with 50% tap water and 50% reverse osmosis water and supplemented with R2 trace element solution at 1:500 (Kieser et al., 2000). Liquid cultures were grown under aeration at 30°C at 250 rpm. MYM agar was supplemented with the following antibiotics when required: 5 µg mL^{-1} kanamycin, 25 µg mL^{-1} hygromycin, or 50 µg mL^{-1} apramycin.

Plasmids and oligos used to generate or verify strains and plasmids are listed in Supplementary File 1, Table 2 and 3, respectively.

Construction and complementation of a *sepH* mutant in *S. venezuelae*

Using 'Redirect' PCR targeting (Gust et al., 2004, 2003), the *sepH* mutant was generated in which the central (1029bp) coding region was replaced with a single apramycin resistance cassette. A cosmid library that covers > 98% of the *S. venezuelae* genome (M.J. Bibb and M.J. Buttner, unpublished) is fully documented at http://strepdb.streptomyces.org.uk/. Cosmid Sv-3-B02 was introduced into *E. coli* BW25113 containing pIJ790 and the *sepH* gene (*vnz_27360*) was replaced with the *apr-oriT* cassette amplified from pIJ773 using the primer pair mb118 and mb119. The resulting disrupted cosmid was confirmed by PCR analysis using the flanking primers mb144 and mb145 and introduced into *S. venezuelae* by conjugation via *E. coli* ET12567/pUZ8002 (Paget et al., 1999). Double cross-over strains (Apr^R, Kan^S) were confirmed by PCR using oligo mb144 and mb145. To avoid any unwanted genetic changes following PCR-targeting and homologous recombination, the Δ*sepH::apr* locus was transduced back into wild-type *S. venezuelae* using the transducing phage SV1 (Stuttard, 1982) as described by Tschowri et al. (Tschowri et al., 2014). A representative transductant (Apr^R) was designated SV56. For complementation, pMB557 was introduced into the *sepH* mutant by conjugation.

Light microscopy and kymograph analysis

For imaging protein localization in *S. venezuelae*, cells were grown in MYM medium for 14-18h and a 2-µL sample of the culture was spotted onto a 1% agarose pad. *Streptomyces* hyphae were visualized using a Zeiss Axio Observer Z.1 inverted epifluorescence microscope fitted with a Zeiss Colibri 7 LED light source and a Zeiss Alpha Plan-Apo 100x/1.46 Oil DIC

M27 objective. Still images and time-lapse images series were collected using Zen Blue (Zeiss) and analyzed using Fiji (Schindelin et al., 2012).

Time-lapse fluorescence imaging *with S. venezuelae* was performed as previously described (Schlimpert et al., 2016). Briefly, *S. venezuelae* strains were grown in MYM medium for about 36 h at 30°C and 250 rpm to reach complete sporulation. To isolate spores, mycelium was pelleted at 400x g for 1 min. Supernatants enriched in spores were diluted in MYM medium to a final concentration of 0.5-5 x 10^7 spores per mL. Spores were loaded into B04A microfluidic plates (ONIX, CellASIC), allowed to germinate and grown by perfusing MYM for 3 h before medium was switched to spent-MYM medium. Spent-MYM was prepared from the 36-hour sporulation culture by filtering the growth medium to remove spores and mycelia fragments. The media flow rate and temperature were maintained at 2 psi and 30°C. Time-lapse imaging was started approximately 8 h after spores had germinated and images were acquired every 10 min until sporulation was completed.

Kymographs were generated from time-lapse image series of strain SS12 (WT/*ftsZ-ypet*) and MB750 (Δ*sepH*/*ftsZ-ypet*) using Fiji (Schindelin et al., 2012). Hyphae undergoing sporulation septation were first identified based on the characteristic FtsZ-YPet localization pattern following the cessation of tip extension. 47 frames (10min/frame) including 12 frames immediately before and 34 frames after the cessation of hyphal growth were isolated. Selected hyphae were "straightened" in Fiji and a segmented line (5pt) was manually drawn along the center of the straightened hyphae. FtsZ-YPet fluorescence intensity was plotted along this line as a function of time (460min) using the "Reslice" command. Kymographs were further annotated in Adobe Illustrator.

Spore length measurements

Lawns of the respective *S. venezuelae* strains were generated by spreading a single colony onto MYM agar. The plates were incubated for 3-4 days at 30°C until sporulation was completed. Spores were washed off the agar using 20% glycerol and a sterile cotton pad through which spores where harvested using a sterile syringe. A small aliquot of the spore suspension was mounted on a microscope slide on top of a thin agarose pad (1% agarose dissolved in water) and imaged by phase-contrast microscopy using a Zeiss Axio Observer Z.1 inverted microscope and a Zeiss Alpha Plan-Apo 100x/1.46 Oil DIC M27 objective. Spore lengths were determined using the software Fiji (Schindelin et al., 2012) except for spore length measurements in Figure 7B in which case the MicrobeJ plug-in for Fiji was used (Ducret et al., 2016).

587 **Staining of DNA and peptidoglycan**

588 *S. venezuelae* wildtype and SV56 cells were grown in confluent patches on MYM agar for 1-
589 2 days. Glass coverslips were gently pressed onto the cell material and removed. Coverslips
590 were fixed with 100% methanol for 1 minute. Sterile H_2O was used to wash the coverslips.
591 Spore chains attached to the coverslips were incubated with the DNA-stain 7-AAD (7-
592 Aminoactinomycin D, 10 µg mL^{-1}) and with Wheat Germ Agglutinin (WGA), Alexa Fluor™ 488
593 Conjugate (50 µg mL^{-1}) to visualize cell wall material. The samples were incubated for 30
594 minutes in the dark, after which the dyes were removed with sterile H_2O. The coverslips were
595 then mounted onto agarose pads and visualized by fluorescence microscopy.

596 For HADA (7-hydroxycoumarin 3-carboxylic acid-amino-D-alanine) labelling (Kuru et al.,
597 2015), spores were loaded into BA04 microfluidic plates (CellASIC ONIX). Trapped spores
598 were continuously supplied with MYM containing 0.25 mM HADA at 2 psi at 30°C. Following
599 spore germination, hyphae were allowed to grow by perfusing MYM-HADA at 2 psi for 4-5
600 hours. Prior to image acquisition MYM-HADA was replaced with MYM and hyphae were
601 visualized using fluorescence microscopy as described above. Images were collected using
602 Zen Blue (Zeiss) and analyzed using Fiji (Schindelin et al., 2012).

603 **Cryo-scanning electron microscopy**

604 *S. venezuelae* colonies were mounted on the surface of an aluminium stub with Tissue Tek™
605 OCT (optimal cutting temperature compound) (Agar Scientific Ltd, Essex, UK), plunged into
606 liquid nitrogen slush at approximately -210°C to cryo-preserve the material, and transferred to
607 the cryo-stage of an Alto 2500 cryotransfer system (Gatan, Oxford, England) attached to either
608 a FEI NanoSEM 450 field emission gun scanning electron microscope (FEI Ltd, Eindhoven,
609 The Netherlands) or a Zeiss Supra 55 field emission gun scanning electron microscope (Zeiss
610 UK Ltd, Cambridge). The surface frost was sublimated at -95°C for 3½ mins before the sample
611 was sputter coated with platinum for 2 min at 10 mA at below -110°C. Finally, the sample was
612 moved onto the cryo-stage in the main chamber of the microscope, held at approximately -
613 130°C, and viewed at 3 kV.

614 **Transmission electron microscopy**

615 FtsZ filament morphology was visualized by negative staining and transmission electron
616 microscopy. For FtsZ from *S. venezuelae*, 3.5 µM FtsZ and/or 3.5 µM SepH was prepared in
617 buffer P (50 mM HEPES pH 7.2, 50 mM KCl, 5 mM $MgCl_2$). All the solutions were previously
618 filtered using 0.1-µm centrifugal filter units (Millipore). Reactions were pre-warmed at 30°C for
619 10 min, started by adding 2 mM GTP and incubated at 30°C for additional 10 min. 3.5 µL of
620 each reaction was placed on a carbon-filmed, 400 mesh copper grid (EM Resolutions,
621 Sheffield, UK) which had been glow discharged for 20 seconds at 10 mA in an Ace 200 (Leica

Microsystems (UK) Ltd, Milton Keynes, UK). After 60 seconds, excess sample was wicked away using Whatman No. 1 filter paper and grids were negatively stained using 2% (w/v) uranyl acetate in water. Grids were imaged using a Talos F200C transmission electron microscope (ThermoFisher Scientific, Eindhoven, The Netherlands) operated at 200 kV, equipped with a 4k OneView CMOS detector (Gatan UK, Abingdon, Oxfordshire, UK).

For *M. smegmatis* proteins, 6 µM $FtsZ_{Ms}$ was prepared in modified buffer P (50 mM HEPES pH 6.8, 100 mM KCl, 5 mM $MgCl_2$) in the absence or presence of $SepH_{Ms}$ at 3 µM or 6 µM. Reactions were pre-warmed to 37°C for 10 min, and then started by adding 2 mM GTP and incubated for further 20min. Samples were stained and imaged as described above.

Measurement of FtsZ filament width

TEM micrographs of FtsZ filaments assembled in the presence or absence of SepH were used to manually estimate filament width. Analysis was performed in Fiji (Schindelin et al., 2012) by extracting the grey values along a line which was drawn perpendicular to the longitudinal axis of FtsZ filaments. Obtained intensity profiles were aligned manually by setting the highest grey values as the centre of the filament and plotted using GraphPad Prism8. The distance between the two lowest grey values was defined as the average width of the FtsZ filaments.

Automated Western blot analysis

For analysis of protein levels, we used the automated capillary-based immunoassay platform WES (ProteinSimple, San Jose, CA). To prepare proteins samples, 2 mL aliquots of liquid MYM cultures were sampled at the desired time points. Mycelium was pelleted by centrifugation and washed with PBS. Pellets were snap-frozen in liquid nitrogen and stored at -80°C until use. Mycelia pellets were thawed on ice and resuspended in 0.4 mL ice-cold lysis buffer (20 mM Tris pH 8.0, 5 mM EDTA, 1x EDTA-free protease inhibitors [Roche]) and sonicated (5x 15 sec on/15 sec off at 5-micron amplitude). Cell lysates were then cleared by centrifugation at 16,000x g for 20 min at 4°C. Total protein concentration was determined using Bradford reagent (Biorad) and 1 µg of total protein was then loaded in technical triplicates into a microplate (ProteinSimple). For the detection of SepH, FtsZ or YPet-fusion proteins anti-SepH antibody (1:200), anti-FtsZ antibody (1:200) or anti-GFP antibody (1:200) was used. Data analysis and the generation of virtual western blots was done using the Compass Software (Protein Simple, Version XZ).

Yeast two-hybrid analysis

The yeast two-hybrid assays were performed in strain *Saccharomyces cerevisiae* Y2HGold (Takara Bio USA). Combination of the two plasmids encoding the desired fusion proteins were transformed into Y2HGold cells using Frozen-EZ Yeast Transformation II Kit (Zymo Research). Selection for growth was carried out on selective drop-out plates lacking leucine

and tryptophan ($SD^{-Leu-Trp}$) and single colonies were inoculated into liquid $SD^{-Leu\ -Trp}$ medium and grown overnight at 30°C. Saturated cultures were diluted 1:4 in water and 5 µL of each dilution was then spotted on $SD^{-Leu-Trp}$ and $SD^{-Leu\ -Trp\ -Ade\ -His}$ (additionally lacking adenine and histidine) in order to test for growth and interaction, respectively. Plates were incubated for 4-5 days at 30°C and scanned. Each interaction was tested in biological triplicate experiments.

Protein expression and purification

To purify untagged SepH, SepH mutant variants and FtsZ from *S. venezuelae* and $FtsZ_{MS}$ from *M. smegmatis*, *E. coli* Rossetta (DE3) was transformed with derivatives of the plasmid pTB146 to produce His_6-SUMO-tagged protein fusions. Cells were grown at 37°C in LB medium containing 50 µg mL^{-1} carbenicillin, 25 µg mL^{-1} chloramphenicol and 1% glucose overnight and then diluted 1/100 in fresh LB medium containing carbenicillin and chloramphenicol. To induce protein production, 0.5 mM IPTG to the culture once cells reached an OD_{600} of 0.5. Cultures were incubated shaking at 30°C for 4 h and then harvested by centrifugation. Cell pellets were resuspended in Tris-FtsZ buffer (50 mM Tris-HCl pH 8.0, 50 mM KCl and 10% glycerol) and lysed by sonication for 10 cycles at 15-micron amplitude, 15 s ON and 30 s OFF. Lysates were centrifuged at 14,000 rpm for 30 min at 4°C to remove cell debris. His_6-SUMO-FtsZ, His_6-SUMO-SepH or His_6-SUMO-$FtsZ_{Ms}$ were purified using an HisTrap column in ÄKTA pure (GE Healthcare) and eluted using an increasing concentration of imidazole. Fractions containing protein were pooled and dialyzed overnight at 4°C against Tris-FtsZ buffer containing 1 mM DTT and His_6-Upl1 protease at a molar ration of 100:1. The cleaved His_6-SUMO tag and His_6-Upl1 protease were then removed by incubation with Ni-NTA affinity agarose beads. The flow-through containing untagged FtsZ, SepH or $FtsZ_{Ms}$ was then concentrated and subjected to size exclusion chromatography on a HiLoad 16/600 Superdex 200 pg column (GE Healthcare) in Tris-FtsZ buffer. Peak protein fractions were pooled and dialyzed overnight against HEPES-FtsZ buffer (50 mM HEPES pH 7.2, 50 mM KCl, 10% glycerol) and subsequently stored at -80°C until further use.

To purify *M. smegmatis* $SepH_{Ms}$-His_6 ($SepH_{Ms}$), *E. coli* Rossetta (DE3) carrying the plasmid pSS561 was induced for protein overexpression and cell lysis was carried out as described above. $SepH_{Ms}$-His_6 was purified from lysates using an HisTrap column in ÄKTA pure (GE Healthcare) and eluted using an increasing concentration of imidazole. Fractions containing the protein were pooled and dialyzed overnight against HEPES-FtsZ buffer (50 mM HEPES pH 7.2, 50 mM KCl, 10% glycerol) and stored at -80°C until use.

Antibody production

To produce antibodies against FtsZ and SepH from *Streptomyces*, untagged FtsZ and SepH-His_6 were overexpressed and purified as described above, and a total amount of 2 mg of

purified protein was sent to Cambridge Research Biochemicals (UK) to be used to raise antibodies in rabbits.

Analytical gel filtration chromatography

Purified SepH, SepH-NTD, SepH-CTD or SepHG79P was prepared at 30 µM in buffer P (50 mM HEPES pH 7.2, 50 mM KCl, 5 mM $MgCl_2$). A 500-µL sample was subjected to size exclusion chromatography on a Superose 12 10/300 GL column (GE Healthcare) in buffer P using an ÄKTA pure (GE Healthcare) at 0.25 mL min^{-1} constant flow. Gel filtration standards (Bio-Rad) included thyroglobulin (MW 670,000), γ-globuline (MW 158,000), ovalbumin (MW 44,000), myoglobin (MW 17,000) and vitamin B12 (MW 1,350). Standards were separated using the same conditions described above, and the retention volume of each of the proteins was plotted against Log MW. The standard curve was used to calculate the molecular weight of SepH using the retention volume previously obtained. The same procedure described above was carried out for $SepH_{Ms}$ but using a modified buffer P (50 mM HEPES pH 6.8, 100 mM KCl, 5 mM $MgCl_2$).

GTPase activity assay

FtsZ GTPase activity was monitored using the PiColorLock Gold kit (Expedeon), a malachite-green-based assay. SepH and FtsZ were diluted to the desired concentration in buffer P (50 mM HEPES pH 7.2, 50 mM KCl, 5 mM $MgCl_2$). The protein solution was incubated for 5 min at 30°C and the reaction was started by adding 50 µM GTP. Samples were taken at 0, 2.5, 5, 7.5 and 10 min. Reactions were stopped by adding an equal volume of 0.6 M perchloric acid. Absorbance at 620 nm was measured and plotted using Microsoft Excel. GTPase activity was determined from the linear range of the curves (Wasserstrom et al., 2013). GTPase activity assays for *M. smegmatis* $FtsZ_{Ms}$ and $SepH_{Ms}$ were performed as described above but using a modified buffer P (50 mM HEPES pH 6.8, 100 mM KCl, 5 mM $MgCl_2$) and incubating the protein solutions at 37°C. Samples were taken at 0, 5, 10, 15 and 20 min and data was analyzed as described above.

Dynamic light scattering

FtsZ assembly was monitored using a Wyatt Dynapro Titan Dynamic Light Scattering (DLS) instrument. All components of the reaction buffer were filtered using 0.1-µm centrifugal filter units (Millipore). *Streptomyces* FtsZ (3.5 µM) was prepared in buffer P (50 mM HEPES pH 7.2, 50 mM KCl, 5 mM $MgCl_2$) and SepH was added at the desired concentrations when required. 15-µL of the resulting protein solution was transferred to a quartz cuvette and equilibrated to 30°C for 5 min in the DLS instrument and the laser intensity adjusted until readings reached ~20,000 counts. Baseline readings were taken for 5 min, GTP (50 µM or 2 mM) was added and light scatter readings were recorded for up to 30 min. The same protocol

was followed in the case of GDP or GMPCCP. Data were visualized using Dynamics software (v6), transferred to an Excel file and plotted using GraphPad Prism. *M. smegmatis* $FtsZ_{Ms}$ (6 µM) was prepared in modified buffer P (50 mM HEPES pH 6.8, 100 mM KCl, 5 mM $MgCl_2$) in the presence or absence of $SepH_{Ms}$ (3 µM). All DLS measurements with *M. smegmatis* proteins were performed at 37°C, baseline readings were first monitored for 5 min, followed by the addition of 2 mM GTP and the recording of the scatter profile for up to 35 min. Data was analyzed as described above.

Circular dichroism spectroscopy

SepH or SepHG79P (3.5 µM) were dialyzed overnight against phosphate buffer pH 7.2 to dilute the sodium ions in preparation for CD analysis. Spectra were recorded in 1 nm steps on a Chirascan Plus spectrophotometer (Applied Photophysics) at 20°C in a 0.5 mm quartz cuvette (Hellma). Measurements were collected in triplicate, averaged and background subtracted with matched buffer using the Chirascan software package. Data were exported to an Excel file and plotted using GraphPad Prism.

Sedimentation assay

FtsZ (3.5 µM) and/or SepH (3.5 µM) were prepared in buffer P (50 mM HEPES pH 7.2, 50 mM KCl, 5 mM $MgCl_2$). Reactions were incubated at 30°C for 10 min and polymerization was started by adding GTP (2mM) or GMPCCP (2 mM). Samples were incubated for an additional 15 min at 30°C and then pelleted by ultracentrifugation at 350,000x g for 15 min (high-speed), or at 25,000x g for 30 min (low-speed). Supernatant and pellet fractions were mixed with equivalent volumes of SDS sample buffer. Proteins were visualized by SDS-PAGE and Coomassie staining and proteins bands were quantified using Fiji (Schindelin et al., 2012).

For *M. smegmatis* proteins, $FtsZ_{Ms}$ (6 µM) and/or $SepH_{Ms}$ (3 µM) were prepared in modified buffer P (50 mM HEPES pH 6.8, 100 mM KCl, 5 mM $MgCl_2$). Reactions were incubated at 37°C for 10 min, started by adding 2 mM GTP final concentration, incubated for an additional 20 min followed by ultracentrifugation and SDS-PAGE analysis as described above.

Chromatin immunoprecipitation and deep-sequencing (ChIP-seq)

Wild-type *S. venezuelae* and the *ΔsepH* mutant (SV56) were grown in four 30-mL volumes of MYM medium for 18h (sporulation). Cross-linking and immunoprecipitation were conducted as described by (Bush et al., 2019) using the anti-SepH polyclonal antibody. Library construction and sequencing were performed by Genewiz (NJ, USA), using Illumina Hiseq (2 x 150 bp configuration, trimmed to 100 bp).

Reads in the fastq files received from the sequencing contractor were aligned to the *S. venezuelae* genome (GenBank accession number CP018074) using the bowtie2 (2) software (version 2.2.9), which resulted in one SAM (.sam) file for each pair of fastq files (paired-end

sequencing). For each SAM file, the depth command of samtools (version 1.8) was used to arrive at the depth of sequencing at each nucleotide position of the *S. venezuelae* chromosome (https://www.sanger.ac.uk/science/tools/samtools-bcftools-htslib). From the sequencing depths at each nucleotide position determined in 2, a local enrichment was calculated in a moving window of 30 nucleotides moving in steps of 15 nucleotides as (the mean depth at each nucleotide position in the 30-nt window) divided by (the mean depth at each nucleotide position in a 3000-nucleotide window cantered around the 30-nucleotide window). This results in an enrichment ratio value for every 15 nucleotides along the genome. The enrichment ratios thus calculated were stored in files in the bedgraph format and were used for viewing in IGB. After ensuring good correlation between the replicates (Spearman correlation coefficient > 0.95) the mean of the replicates was calculated and used in further calculations. Enrichment in the control was subtracted from the enrichment in the WT files. Significance of enrichment was calculated assuming normal distribution of the control-subtracted enrichment values. The SepH ChIP-seq data has been deposited at the MIAME-compliant ArrayExpress database (https://www.ebi.ac.uk/arrayexpress/) under accession number E-MTAB-9064.

DNase I footprinting

DNase I footprinting experiments were carried out essentially as previously described (Bush et al., 2013) and according to the manufacturer's instructions (Sure Track footprinting kit, Amersham Pharmacia Biotech). DNA fragments from the promoter regions of *vnz35870, vnz30075* and *vnz07520* were amplified by PCR from the PL1_M15, PL1_G3 and PL1_E16 cosmids, using the primer pairs mb1136/mb1129, mb1138/mb1139 and mb1140/mb1133, respectively. Oligonucleotides were first end-labelled with T4 polynucleotide kinase (Amersham Pharmacia Biotech) and [γ-32P]-ATP as described by the manufacturer. Binding reactions were carried out at room temperature for 30 min in 1x Polymerization Buffer (50mM HEPES/KOH pH7.2, 50 mM KCl, 5 mM $MgCl_2$) in a total volume of 40 µL, and in the presence of approximately 50000-75000 cpm of the DNA probe. Following incubation, 10 µL containing 3 units of DNase I (Promega) and 1 µL of $CaCl_2$ was added, mixed and incubated for 1 min. The reaction was stopped by addition of 140 µL stop solution [192 mM NaAc, 32 mM EDTA, 0.14% SDS, 70 µg yeast-tRNA (Invitrogen)]. Samples were then phenol-chloroform extracted prior to ethanol (96%) precipitation. The pellet was vacuum-dried and resuspended in 5 µL of formamide loading dye (95% formamide, 20 mM EDTA pH 8.0, 0.1% bromophenol blue, 0.1% xylene cyanol FF). 2.5 µL of each sample was loaded on a 6% sequencing gel, next to a G+A ladder, prepared according to the Sure Track footprinting kit (Amersham Pharmacia Biotech). The gel was then vacuum-dried before imaging using image plates, visualized using the FUJIFILM FLA-7000.

798 **Electrophoretic mobility-shift assay (EMSA)**

799 DNA sequences were amplified by PCR using the primer pairs mb1136/mb1129,
800 mb1124/mb1125, mb1126/mb1127 and the templates PL1_M15, SV-4-G01 and pCOLADuet-
801 1 respectively. This generated probes to test for potential binding of SepH to the promoter
802 region of *vnz35870*, a sequence internal to *vnz08520* (*ftsZ*) and a low-GC sequence from the
803 vector *kan*^{R}-gene (*aphII*). Binding reactions were carried out at room temperature for 30 min
804 in 1x Polymerization Buffer (50 mM HEPES/KOH pH7.2, 50 mM KCl, 5 mM $MgCl_2$) in a total
805 volume of 20 µL, and in the presence of 50 ng of the DNA probe. Following the incubation
806 step, samples were run on pre-cast Mini-PROTEAN TBE gels (Bio-Rad 456-5014) in 0.5 x
807 TBE for 60-90 min alongside 100 bp ladder (NEB). Gels were stained for 30 minutes in
808 ethidium bromide solution before imaging under UV-light.

809 **Phylogenetics analysis**

810 The SepH sequence from *Streptomyces venezuelae* (vnz27360) was used to BLAST against
811 3962 representative bacterial species (Altschul et al., 1997, 1990; Camacho et al., 2009). After
812 reciprocal BLAST analysis and quality filtering, 626 actinobacterial SepH homologs were
813 identified. The 626 sequences were clustered to remove redundancies using CD-HIT at 90%
814 similarity and then clustered again at 75% similarity to reduce the likelihood of misclustering
815 (Li and Godzik, 2006). These representative homologs (360 sequences) were used to created
816 three separate sequence alignments using CLUSTALX (Larkin et al., 2007), MUSCLE (Edgar,
817 2004a, 2004b), and MAFFT, using the l-ins-I option (Katoh and Standley, 2014). TrimAl was
818 used to compare the alignments for consistency, at which point the most consistent
819 (CLUSTAL) was used and gaps that were present in 80% or more of sequences, were trimmed
820 out (Capella-Gutiérrez et al., 2009). This alignment was used to generate a tree in PHYML
821 (Guindon et al., 2010) using the model, LG +G, as selected by SMS (Lefort et al., 2017). The
822 tree was visualized using iTOL, the Interactive Tree of Life (Letunic and Bork, 2019).
823 Additionally, the alignment was used to generate a logo using WebLogo3 (Crooks et al., 2004).

824

825 **Acknowledgments**

826 We would like to thank Clare Stevenson and Julia Mundy for technical assistance and advice
827 and Kelley Gallagher for helpful discussions on the phylogenetic analysis. We thank the JIC
828 Bioimaging facility and staff for technical support. Work in the lab of JRM was supported by
829 the National Institutes of Health grant GM096268. We gratefully acknowledge funding by the
830 Royal Society (URF\R1\180075) and the BBSRC (BB/T015349/1) to SS and for support by
831 the BBSRC Institute Strategic Program grant BB/J004561/1 to the John Innes Centre.

832

833 **Competing interests**

834 The authors declare that no competing interests exist.

References

Altschul SF, Gish W, Miller W, Myers EW, Lipman DJ. 1990. Basic local alignment search tool. *Journal of Molecular Biology* **215**:403–410. doi:10.1016/S0022-2836(05)80360-2

Altschul SF, Madden TL, Schäffer AA, Zhang J, Zhang Z, Miller W, Lipman DJ. 1997. Gapped BLAST and PSI-BLAST: a new generation of protein database search programs. *Nucleic Acids Research* **25**:3389–3402. doi:10.1093/nar/25.17.3389

Aravind L, Anantharaman V, Balaji S, Babu MM, Iyer LM. 2005. The many faces of the helix-turn-helix domain: transcription regulation and beyond. *FEMS Microbiol Rev* **29**:231–262. doi:10.1016/j.femsre.2004.12.008

Barka EA, Vatsa P, Sanchez L, Gaveau-Vaillant N, Jacquard C, Meier-Kolthoff JP, Klenk H-P, Clément C, Ouhdouch Y, van Wezel GP. 2016. Taxonomy, Physiology, and Natural Products of Actinobacteria. *Microbiol Mol Biol Rev* **80**:1–43. doi:10.1128/MMBR.00019-15

Bisson-Filho AW, Hsu Y-P, Squyres GR, Kuru E, Wu F, Jukes C, Sun Y, Dekker C, Holden S, VanNieuwenhze MS, Brun YV, Garner EC. 2017. Treadmilling by FtsZ filaments drives peptidoglycan synthesis and bacterial cell division. *Science* **355**:739–743. doi:10.1126/science.aak9973

Bush MJ, Bibb MJ, Chandra G, Findlay KC, Buttner MJ. 2013. Genes required for aerial growth, cell division, and chromosome segregation are targets of WhiA before sporulation in *Streptomyces venezuelae*. *mBio* **4**. doi:10.1128/mBio.00684-13

Bush MJ, Chandra G, Al-Bassam MM, Findlay KC, Buttner MJ. 2019. BldC delays entry into development to produce a sustained period of vegetative growth in *Streptomyces venezuelae. mBio* **10**. doi:10.1128/mBio.02812-18

Bush MJ, Chandra G, Bibb MJ, Findlay KC, Buttner MJ. 2016. Genome-wide chromatin immunoprecipitation sequencing analysis shows that WhiB is a transcription factor that cocontrols its regulon with WhiA to initiate developmental cell division in *Streptomyces*. *MBio* **7**:e00523-00516. doi:10.1128/mBio.00523-16

Bush MJ, Tschowri N, Schlimpert S, Flärdh K, Buttner MJ. 2015. c-di-GMP signalling and the regulation of developmental transitions in streptomycetes. *Nature Reviews Microbiology* **13**:749–760. doi:10.1038/nrmicro3546

Caldas P, López-Pelegrín M, Pearce DJG, Budanur NB, Brugués J, Loose M. 2019. Cooperative ordering of treadmilling filaments in cytoskeletal networks of FtsZ and its crosslinker ZapA. *Nature Communications* **10**:5744. doi:10.1038/s41467-019-13702-4

Camacho C, Coulouris G, Avagyan V, Ma N, Papadopoulos J, Bealer K, Madden TL. 2009. BLAST+: architecture and applications. *BMC Bioinformatics* **10**:421. doi:10.1186/1471-2105-10-421

Capella-Gutiérrez S, Silla-Martínez JM, Gabaldón T. 2009. trimAl: a tool for automated alignment trimming in large-scale phylogenetic analyses. *Bioinformatics* **25**:1972–1973. doi:10.1093/bioinformatics/btp348

Crooks GE, Hon G, Chandonia J-M, Brenner SE. 2004. WebLogo: a sequence logo generator. *Genome Res* **14**:1188–1190. doi:10.1101/gr.849004

Ducret A, Quardokus EM, Brun YV. 2016. MicrobeJ, a tool for high throughput bacterial cell detection and quantitative analysis. *Nat Microbiol* **1**:16077. doi:10.1038/nmicrobiol.2016.77

Edgar RC. 2004a. MUSCLE: multiple sequence alignment with high accuracy and high throughput. *Nucleic Acids Res* **32**:1792–1797. doi:10.1093/nar/gkh340

Edgar RC. 2004b. MUSCLE: a multiple sequence alignment method with reduced time and space complexity. *BMC Bioinformatics* **5**:113. doi:10.1186/1471-2105-5-113

Eswara PJ, Brzozowski RS, Viola MG, Graham G, Spanoudis C, Trebino C, Jha J, Aubee JI, Thompson KM, Camberg JL, Ramamurthi KS. 2018. An essential *Staphylococcus aureus* cell division protein directly regulates FtsZ dynamics. *Elife* **7**. doi:10.7554/eLife.38856

884 Gao B, Paramanathan R, Gupta RS. 2006. Signature proteins that are distinctive characteristics of
885 Actinobacteria and their subgroups. *Antonie Van Leeuwenhoek* **90**:69–91.
886 doi:10.1007/s10482-006-9061-2
887 García-Soriano DA, Heermann T, Raso A, Rivas G, Schwille P. 2020. The speed of FtsZ treadmilling is
888 tightly regulated by membrane binding. *Scientific Reports* **10**:10447. doi:10.1038/s41598-020-
889 67224-x
890 Griffin JE, Gawronski JD, Dejesus MA, Ioerger TR, Akerley BJ, Sassetti CM. 2011. High-resolution
891 phenotypic profiling defines genes essential for mycobacterial growth and cholesterol
892 catabolism. *PLoS Pathog* **7**:e1002251. doi:10.1371/journal.ppat.1002251
893 Guindon S, Dufayard J-F, Lefort V, Anisimova M, Hordijk W, Gascuel O. 2010. New algorithms and
894 methods to estimate maximum-likelihood phylogenies: assessing the performance of PhyML
895 3.0. *Syst Biol* **59**:307–321. doi:10.1093/sysbio/syq010
896 Gust B, Challis GL, Fowler K, Kieser T, Chater KF. 2003. PCR-targeted *Streptomyces* gene replacement
897 identifies a protein domain needed for biosynthesis of the sesquiterpene soil odor geosmin |
898 PNAS. *Proceedings of the National Academy of Sciences* **100**:1541–1546.
899 Gust B, Chandra G, Jakimowicz D, Yuqing T, Bruton CJ, Chater KF. 2004. λ Red-mediated genetic
900 manipulation of antibiotic-producing *Streptomyces* - ScienceDirect. *Advances in Applied*
901 *Microbiology* **54**:107–128.
902 Katoh K, Standley DM. 2014. MAFFT: iterative refinement and additional methods. *Methods Mol Biol*
903 **1079**:131–146. doi:10.1007/978-1-62703-646-7_8
904 Kieser T, Bibb MJ, Buttner MJ, Chater KF, Hopwood DA. 2000. Practical *Streptomyces* Genetics. John
905 Innes Foundation.
906 Kuru E, Tekkam S, Hall E, Brun YV, Van Nieuwenhze MS. 2015. Synthesis of fluorescent D-amino acids
907 and their use for probing peptidoglycan synthesis and bacterial growth in situ. *Nat Protoc*
908 **10**:33–52. doi:10.1038/nprot.2014.197
909 Larkin MA, Blackshields G, Brown NP, Chenna R, McGettigan PA, McWilliam H, Valentin F, Wallace IM,
910 Wilm A, Lopez R, Thompson JD, Gibson TJ, Higgins DG. 2007. Clustal W and Clustal X version
911 2.0. *Bioinformatics* **23**:2947–2948. doi:10.1093/bioinformatics/btm404
912 Lefort V, Longueville J-E, Gascuel O. 2017. SMS: Smart Model Selection in PhyML. *Mol Biol Evol*
913 **34**:2422–2424. doi:10.1093/molbev/msx149
914 Letunic I, Bork P. 2019. Interactive Tree Of Life (iTOL) v4: recent updates and new developments.
915 *Nucleic Acids Res* **47**:W256–W259. doi:10.1093/nar/gkz239
916 Li W, Godzik A. 2006. Cd-hit: a fast program for clustering and comparing large sets of protein or
917 nucleotide sequences. *Bioinformatics* **22**:1658–1659. doi:10.1093/bioinformatics/btl158
918 Loose M, Mitchison TJ. 2014. The bacterial cell division proteins FtsA and FtsZ self-organize into
919 dynamic cytoskeletal patterns. *Nat Cell Biol* **16**:38–46. doi:10.1038/ncb2885
920 McCormick JR. 2009. Cell division is dispensable but not irrelevant in *Streptomyces*. *Curr Opin*
921 *Microbiol* **12**:689–698. doi:10.1016/j.mib.2009.10.004
922 McCormick JR, Su EP, Driks A, Losick R. 1994. Growth and viability of *Streptomyces coelicolor* mutant
923 for the cell division gene *ftsZ*. *Mol Microbiol* **14**:243–254. doi:10.1111/j.1365-
924 2958.1994.tb01285.x
925 McQuillen R, Xiao J. 2020. Insights into the structure, function, and dynamics of the bacterial
926 cytokinetic FtsZ-ring. *Annual Review of Biophysics* **49**:309–341. doi:10.1146/annurev-biophys-
927 121219-081703
928 Mercy C, Ducret A, Slager J, Lavergne J-P, Freton C, Nagarajan SN, Garcia PS, Noirot-Gros M-F, Dubarry
929 N, Nourikyan J, Veening J-W, Grangeasse C. 2019. RocS drives chromosome segregation and
930 nucleoid protection in *Streptococcus pneumoniae*. *Nat Microbiol*. doi:10.1038/s41564-019-
931 0472-z
932 Monteiro JM, Pereira AR, Reichmann NT, Saraiva BM, Fernandes PB, Veiga H, Tavares AC, Santos M,
933 Ferreira MT, Macário V, Van Nieuwenhze MS, Filipe SR, Pinho MG. 2018. Peptidoglycan

synthesis drives an FtsZ-treadmilling-independent step of cytokinesis. *Nature* **554**:528–532. doi:10.1038/nature25506

Paget MSB, Chamberlin L, Atrih A, Foster SJ, Buttner MJ. 1999. Evidence that the extracytoplasmic function sigma factor σE Is required for normal cell wall structure in *Streptomyces coelicolor* A3(2). *J BACTERIOL* **181**:8.

Perez AJ, Cesbron Y, Shaw SL, Villicana JB, Tsui H-CT, Boersma MJ, Ye ZA, Tovpeko Y, Dekker C, Holden S, Winkler ME. 2019. Movement dynamics of divisome proteins and PBP2x:FtsW in cells of Streptococcus pneumoniae. *PNAS* **116**:3211–3220. doi:10.1073/pnas.1816018116

Salerno P, Larsson J, Bucca G, Laing E, Smith CP, Flärdh K. 2009. One of the two genes encoding nucleoid-associated HU proteins in *Streptomyces coelicolor* is developmentally regulated and specifically involved in spore maturation. *J Bacteriol* **191**:6489–6500. doi:10.1128/JB.00709-09

Santos-Beneit F, Roberts DM, Cantlay S, McCormick JR, Errington J. 2017. A mechanism for FtsZ-independent proliferation in *Streptomyces*. *Nat Commun* **8**:1378. doi:10.1038/s41467-017-01596-z

Sassetti CM, Boyd DH, Rubin EJ. 2003. Genes required for mycobacterial growth defined by high density mutagenesis. *Mol Microbiol* **48**:77–84. doi:10.1046/j.1365-2958.2003.03425.x

Schindelin J, Arganda-Carreras I, Frise E, Kaynig V, Longair M, Pietzsch T, Preibisch S, Rueden C, Saalfeld S, Schmid B, Tinevez J-Y, White DJ, Hartenstein V, Eliceiri K, Tomancak P, Cardona A. 2012. Fiji: an open-source platform for biological-image analysis. *Nat Methods* **9**:676–682. doi:10.1038/nmeth.2019

Schlimpert S, Flärdh K, Buttner MJ. 2016. Fluorescence time-lapse imaging of the complete *S. venezuelae* life cycle using a microfluidic device. *J Vis Exp*. doi:10.3791/53863

Schlimpert S, Wasserstrom S, Chandra G, Bibb MJ, Findlay KC, Flärdh K, Buttner MJ. 2017. Two dynamin-like proteins stabilize FtsZ rings during *Streptomyces* sporulation. *Proc Natl Acad Sci USA* **114**:E6176–E6183. doi:10.1073/pnas.1704612114

Sen BC, Wasserstrom S, Findlay K, Söderholm N, Sandblad L, von Wachenfeldt C, Flärdh K. 2019. Specific amino acid substitutions in β strand S2 of FtsZ cause spiraling septation and impair assembly cooperativity in *Streptomyces spp*. *Mol Microbiol* **112**:184–198. doi:10.1111/mmi.14262

Silber N, Mayer C, Opitz CLM de, Sass P. 2020. Antibiotic-induced degradation of FtsZ reveals distinct stages of *Bacillus subtilis* FtsZ ring assembly and constriction. *bioRxiv* 2020.06.30.180018. doi:10.1101/2020.06.30.180018

Squyres GR, Holmes MJ, Barger SR, Pennycook BR, Ryan J, Yan VT, Garner EC. 2020. Dynamics of bacterial cell division: Z ring condensation is essential for cytokinesis. *bioRxiv* 2020.06.30.180737. doi:10.1101/2020.06.30.180737

Stuttard C. 1982. Temperate Phages of *Streptomyces venezuelae*: Lysogeny and host specificity shown by phages SV1 and SV2. *Microbiology,* **128**:115–121. doi:10.1099/00221287-128-1-115

Tschowri N, Schumacher MA, Schlimpert S, Chinnam N babu, Findlay KC, Brennan RG, Buttner MJ. 2014. Tetrameric c-di-GMP Mediates Effective Transcription Factor Dimerization to Control *Streptomyces* Development. *Cell* **158**:1136–1147. doi:10.1016/j.cell.2014.07.022

van den Ent F, Johnson CM, Persons L, de Boer P, Löwe J. 2010. Bacterial actin MreB assembles in complex with cell shape protein RodZ. *The EMBO Journal* **29**:1081–1090. doi:10.1038/emboj.2010.9

Wasserstrom S, Grantcharova N, Ubhayasekera W, Ausmees N, Sandblad L, Flardh K. 2013. Non-sporulating ftsZ mutants in *Streptomyces coelicolor* reveal amino acid residues critical for FtsZ polymerization dynamics. *Microbiology* **159**:890–901. doi:10.1099/mic.0.066480-0

White EL, Ross LJ, Reynolds RC, Seitz LE, Moore GD, Borhani DW. 2000. Slow polymerization of *Mycobacterium tuberculosis* FtsZ. *Journal of Bacteriology* **182**:4028–4034. doi:10.1128/JB.182.14.4028-4034.2000

985 Whitley KD, Jukes C, Tregidgo N, Karinou E, Almada P, Henriques R, Dekker C, Holden S. 2020. FtsZ
986 treadmilling is essential for Z-ring condensation and septal constriction initiation in bacterial
987 cell division. *bioRxiv* 2020.07.01.182006. doi:10.1101/2020.07.01.182006
988 Willemse J, Borst JW, Waal E de, Bisseling T, Wezel GP van. 2011. Positive control of cell division:
989 FtsZ is recruited by SsgB during sporulation of *Streptomyces*. *Genes Dev* **25**:89–99.
990 doi:10.1101/gad.600211
991 Woldemeskel S, McQuillen R, Hessel AM, Xiao J, Goley ED. 2017. A Conserved Coiled-Coil Protein Pair
992 Focuses the Cytokinetic Z-Ring in *Caulobacter crescentus*. *Mol Microbiol* **105**:721–740.
993 doi:10.1111/mmi.13731
994 Yang X, Lyu Z, Miguel A, McQuillen R, Huang KC, Xiao J. 2017. GTPase activity-coupled treadmilling of
995 the bacterial tubulin FtsZ organizes septal cell wall synthesis. *Science* **355**:744–747.
996 doi:10.1126/science.aak9995

1 Figure 1

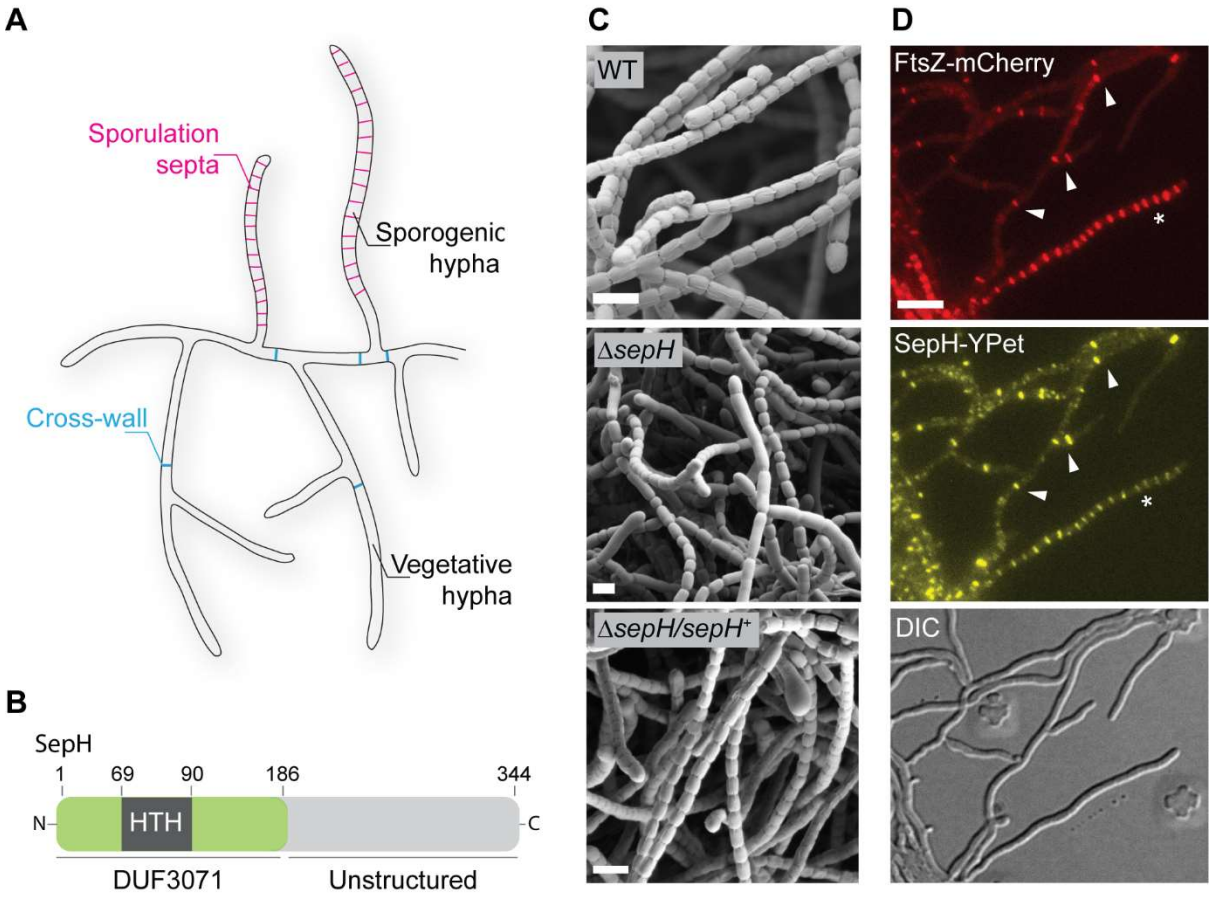

2

3 **Figure 1. SepH is required for sporulation septation in *Streptomyces venezuelae*. (A)**
4 Schematic illustrating the multicellular lifestyle of *Streptomyces* including the two FtsZ-
5 dependent modes of cell division that occur in vegetative and sporogenic hyphae: cross-wall
6 formation and sporulation septation. **(B)** Schematic of the predicted SepH domain
7 organization, including the N-terminal DUF3071 domain containing a helix-turn-helix motif
8 (HTH), and the unstructured C-terminal domain. Numbers indicate corresponding amino acid
9 positions. **(C**) Cryo-scanning electron micrographs of sporogenic hyphae from wild-type *S.*
10 *venezuelae* (WT), the Δ*sepH* mutant (SV56) and the complemented mutant strain
11 Δ*sepH/sepH*$^+$ (MB747). Scale bars: 2 μm. **(D)** Subcellular co-localization of fluorescently
12 labelled FtsZ (FtsZ-mCherry) and SepH (SepH-YPet) in vegetative and sporulating hyphae.
13 Fluorescent gene fusions were expressed in the wildtype background (MB751). White arrow
14 heads point at cross-walls in vegetative hyphae and the asterisk denotes a sporogenic hypha
15 undergoing sporulation septation. Scale bar: 5 μm.
16

Figure supplement 1. Identification of SepH by ChIP-seq.

Figure supplement 2. Spore length analysis.

Figure supplement 2-source data 1. Spore size measurement data.

Figure supplement 3. Localization and corresponding protein abundance of SepH-YPet in the wildtype and the Δ*ftsZ* mutant.

26 Figure 2

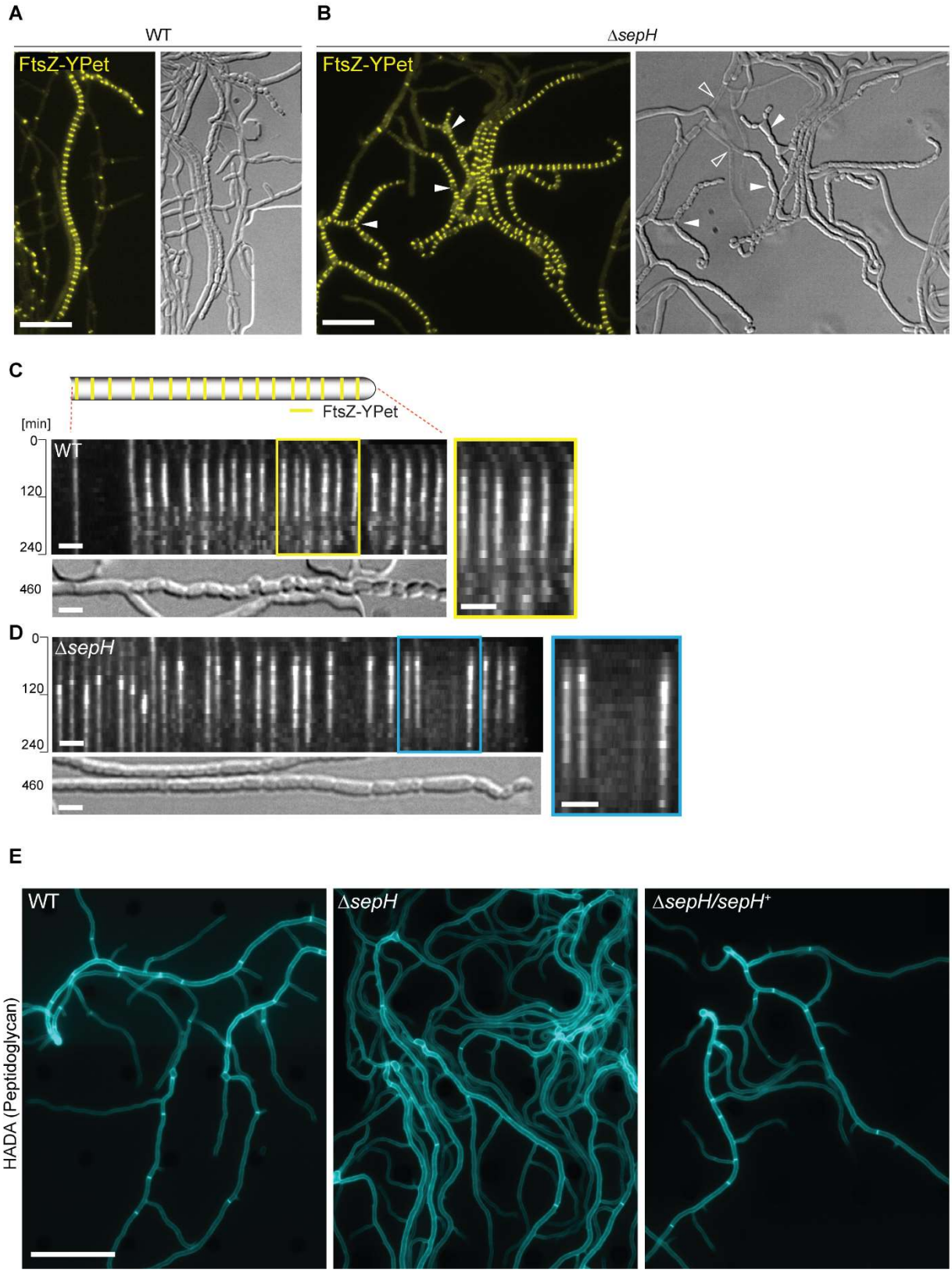

27

28

29 **Figure 2: SepH is important for cell division leading to sporulation septa and cross-**

30 **walls. (A)** and **(B)** Still images from the Supplementary Movie 1 and 2 showing the localization

of FtsZ-YPet in sporulating (A) wildtype (SS12) and (B) Δ*sepH* mutant hyphae (MB750). Arrow heads in (B) point at aberrant spores or gaps in FtsZ-YPet-ladders (filled arrow head) or indicate lysed hyphae (open arrow heads in DIC image). Note that DIC images correspond to a later time point than fluorescence micrographs to show the terminal sporulation phenotype. Scale bars: 10 µm. **(C)** and **(D)** Kymograph analysis of FtsZ-YPet dynamics during sporulation-specific cell division in wildtype (C) and *ΔsepH* cells (D), expressing a *ftsZ-ypet* fusion (SS12 and MB750). The DIC image below shows the resulting spore chain at the end of the experiment. Yellow and blue boxes indicate magnified regions of the kymograph. Scale bar: 2 µm. Additional examples of kymographs can be found in Figure supplement 1 **(E)** HADA staining to visualize cross-walls in wildtype (WT), Δ*sepH* (SV56) and Δ*sepH/sepH*$^{+}$ (MB747) hyphae. Spores of each strains were germinated and grown in the presence of 0.25 mM HADA for 5h in a microfluidic device before imaging. Scale bar: 20 µm.

Source Data 1. Time-lapse fluorescence image series of selected and straightened hyphae (SS12) used to generate kymograph shown in Figure 1C.

Source Data 2. Time-lapse fluorescence image series of selected and straightened hyphae (MB750) used to generate kymograph shown in Figure 1D.

Figure supplement 1. Additional examples of kymographs shown in Figure 2C and D.

Figure supplement 2. FtsZ levels in wildtype and Δ*sepH* cells during sporulation.

Supplementary Movie 1. Time-lapse fluorescence microscopy and DIC image series showing FtsZ-YPet localization in wild-type *S. venezuelae* (SS12).

Supplementary Movie 2. Time-lapse fluorescence microscopy and DIC image series showing FtsZ-YPet localization in the Δ*sepH* mutant (MB750).

Figure 3

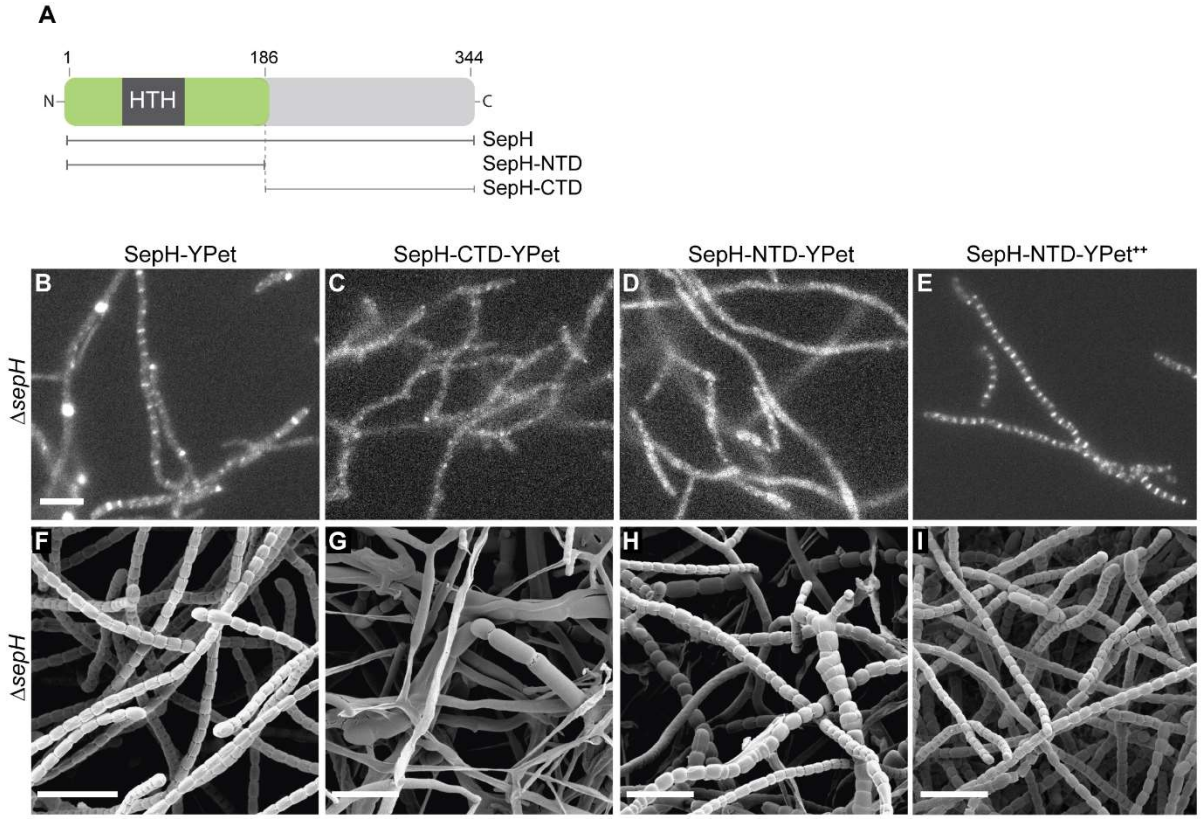

Figure 3: The DUF3071 domain is crucial for SepH function *in vivo*. (A) Schematic showing the SepH domain architecture and constructed truncations. Numbers indicate the relevant amino acid positions. **(B) to (E)** Fluorescence micrographs showing the localization of the full-length and truncated SepH-YPet mutant variants in the Δ*sepH* mutant expressed from the native promoter (B-D, strains MB918, MB827, MB828) or from a constitutive promotor (E, strain MB852). Scale bar: 5 µm. **(F) to (I)** Cryo-SEM images of the same strains presented in (B)-(E) showing the ability of (F) full-length SepH-YPet or (G)-(I) truncated versions of SepH fused to YPet to complement the sporulation defect of the Δ*sepH* mutant (MB918, MB827, MB828 and MB852). Scale bars: 5 µm.

Figure supplement 1. Automated Western blot analysis of SepH-YPet constructs shown in Figure 3B-D.

Figure supplement 2. Cryo-SEM image of the control strain Δ*sepH* carrying the empty vector.

Figure 4

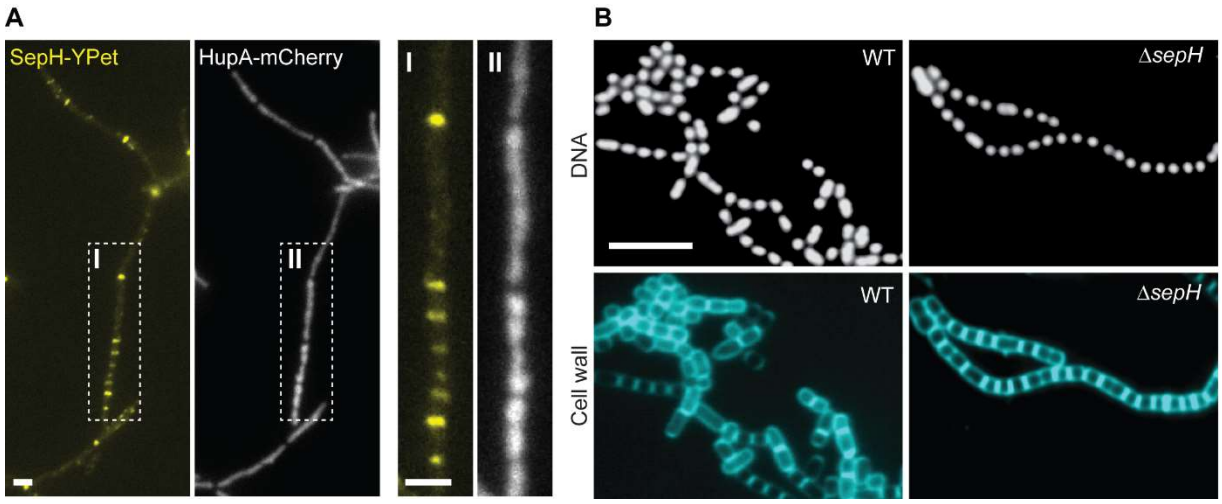

Figure 4: SepH is not associated with the nucleoid or required for chromosome segregation. (A) Fluorescence micrographs showing the accumulation of SepH-YPet and concomitantly distribution of chromosomal DNA using the nucleoid-associated protein HupA fused to mCherry (MB807). Box I and II indicate an enlarged hyphal segment shown in the left panels. Scale bars: 2 µm. **(B)** Fluorescence images of wild-type (WT) and Δ*sepH* (SV56) spore chains incubated with the fluorescent dyes 7AA and WGA Alexa Fluor 488 to visualize DNA and cell wall material, respectively. Scale bar: 5 µm.

Figure supplement 1. Additional results showing the absence of DNA binding by SepH.

Figure 5

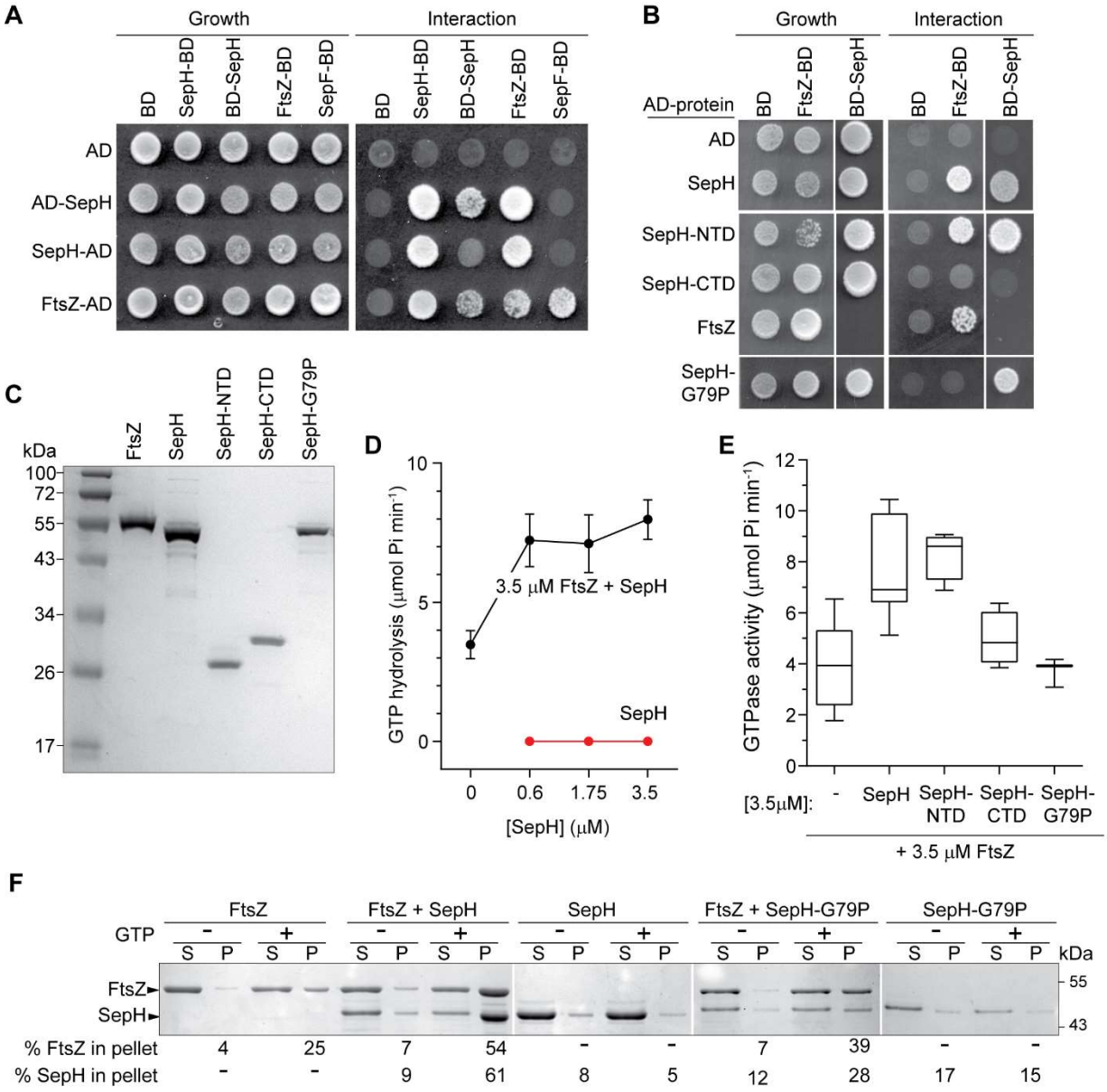

Figure 5: SepH helix-turn-helix motif is crucial for the interaction with FtsZ. (A) Yeast two-hybrid analysis. The indicated proteins were fused to the GAL4 activation domain (AD) and the GAL4 DNA-binding domain (BD). The viability of the yeast strains expressing the respective fusion proteins was confirmed by spotting the individual strains on minimal medium containing leucine and tryptophan (left panel). Interaction between the protein fusion allows growth on minimal medium lacking leucine, tryptophan, histidine and alanine (right panel). The full set of tested interactions can be found in Figure supplement 1. Each interaction was tested in triplicate. **(B)** Yeast two-hybrid assay showing the interaction between FtsZ and different SepH mutant variants, including full-length SepH (SepH), N-terminal domain of SepH (SepH-NTD), C-terminal SepH domain (SepH-CTD) and the mutated SepH helix-turn-helix domain (SepH-G79P). Experiments were performed as described above. **(C)** Coomassie-stained

SDS-PAGE with purified *S. venezuelae* FtsZ, SepH, SepH-NTD (residues 1-186), SepH-CTD (residues 187 to 344) and SepH-G79P. **(D)** Mean GTP hydrolysis rate of 3.5 µM FtsZ alone or in the presence of increasing concentrations of SepH. SepH did not show GTPase activity (red graph). Error bars represent SEM (n≥3) **(E)** Mean GTP hydrolysis rate of FtsZ (3.5 µM) in the presence of wild-type SepH and SepH mutant variants at a molar ratio of 1:1. Error bars represent Min/Max values (n≥3) **(F)** Co-sedimentation of SepH with polymerized FtsZ *in vitro*. 3.5 µM FtsZ was incubated in the presence or absence of 2 mM GTP, and 3.5 µM SepH or SepH-G79P as indicated. Polymerized FtsZ was then collected by high-speed ultracentrifugation. The presence of proteins in the supernatant (S) and pellet (P) was then analyzed by SDS-PAGE and Coomassie staining. The average percentage of total FtsZ or SepH/SepHG79P in the pellet fraction derived from two independent experiments is indicated below.

Figure supplement 1. Y2H analysis of SepH and additional divisome components**.**

Figure supplement 2. Cryo-SEM image of Δ*sepH* complemented with *sepH-G79P*.

Figure supplement 3. Biochemical characterization of SepH and SepH mutant variants with FtsZ.

Figure supplement 4. Low-speed co-sedimentation.

Source Data 1. High-speed co-sedimentation data used in Figure 5F.

Figure supplement 3B-source data 1. Analytical gel filtration data.

Figure supplement 4-source data 2. Low-speed co-sedimentation data.

Figure 6

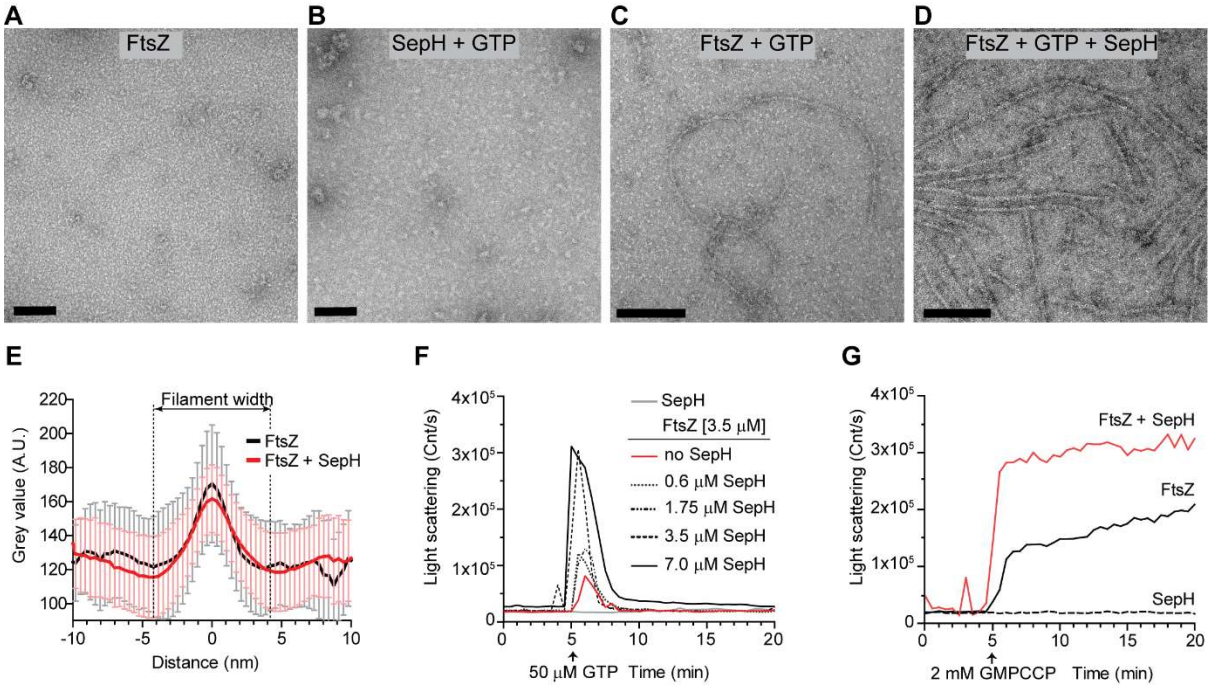

Figure 6: SepH stimulates the polymerization of dynamic FtsZ protofilaments. (A-D) Visualization of purified FtsZ and/or SepH using negative staining transmission electron microscopy (TEM). No structures were detected for 3.5 μM FtsZ in the absence of GTP (A), or 3.5 μM SepH in the presence of GTP (B). Filaments were observed for FtsZ (3.5 μM) when 2mM GTP was added (C), and increased FtsZ polymerization was observed when SepH (3.5 μM) was added to the reaction (D). Scale bar: 100 nm. **(E)** Graph showing the width of FtsZ filaments assembled in the absence (black line, n=59) and presence of SepH (red, n=63) based on the average intensity profile of grey values along a line drawn perpendicular to the longitudinal axis of the filaments where the highest value corresponds to the center of the filaments (0 nm). Error bars represent SD. **(F)** Light scatter traces showing the reversible assembly of 3.5 μM FtsZ filaments in the presence of 50 μM GTP and increasing amounts of SepH. **(G)** Light scatter profile showing the polymerization of 3.5 μM FtsZ with 2 mM GMPCCP in the presence (red line) or absence of 3.5 μM SepH (black line). SepH alone did not generate light scattering when incubated with 2 mM GMPCCP (dashed line). Light scatter graphs display representative traces of at least 3 independent experiments.

Source Data 1. FtsZ filament measurements used to generate Figure 6E.

Figure supplement 1. TEM images of polymerized FtsZ with SepH mutant variants.

Figure supplement 2. Additional DLS results, including control reactions with GDP, SepH mutant variants and 2 mM GTP.

Figure supplement 3. TEM images of FtsZ filaments in the presence of GMPCCP and SepH.

142 Figure 7

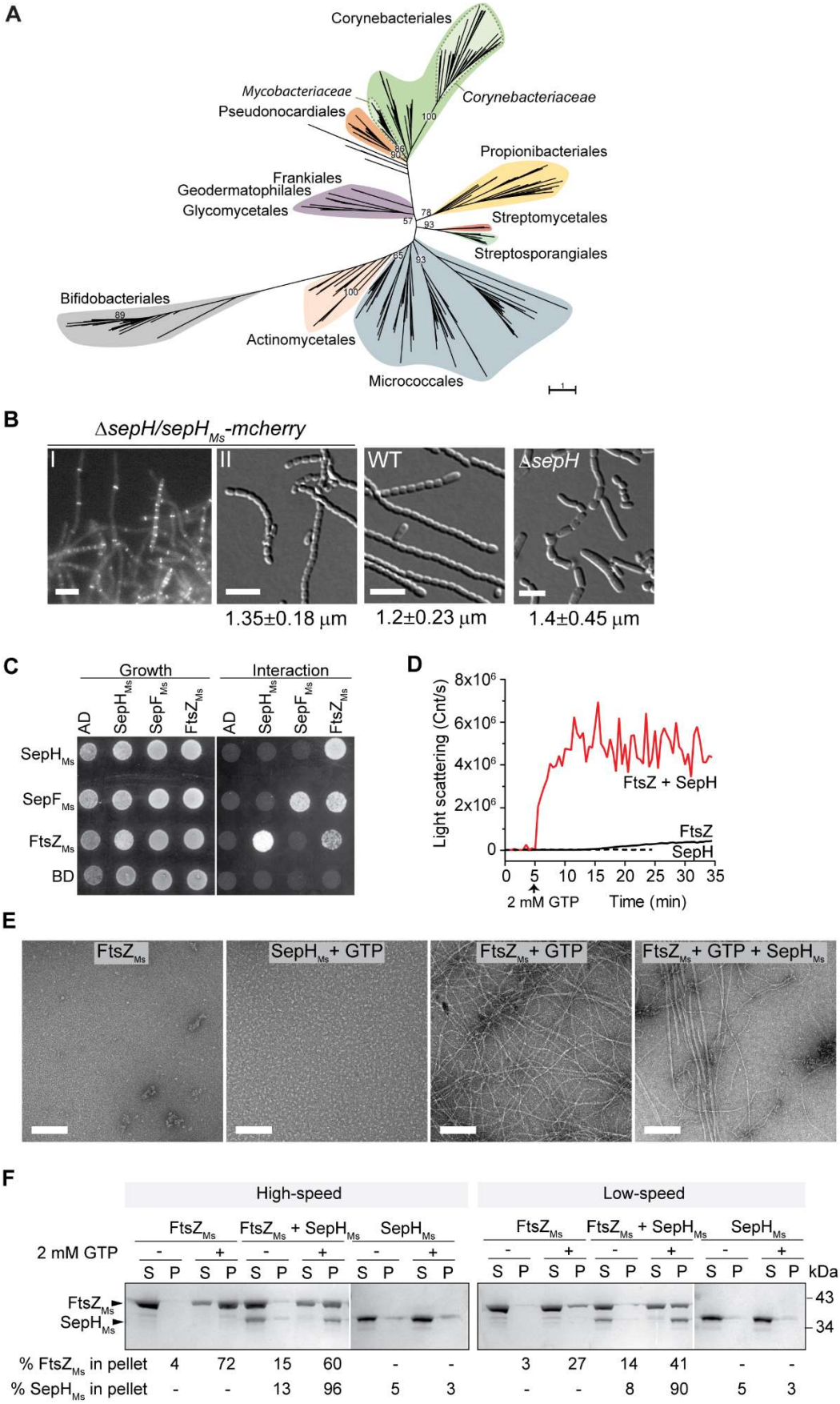

143

Figure 7: $SepH_{Ms}$ stimulates FtsZ polymerization and bundling *in vitro*. **(A)** Phylogenetic tree showing the distribution of SepH within different actinobacterial orders. Major orders with more than two representative leaves are shown in different colors. Numbers denote bootstrap values. The scale bar represents the average substitutions per site. **(B)** Representative fluorescence and DIC images showing the subcellular localization (I) and wildtype-like sporulation (II) of the *S. venezuelae* Δ*sepH* mutant producing $SepH_{Ms}$-mCherry (SS380). For comparison spore chains of the wildtype and the Δ*sepH* mutant (SV56) are shown and the mean ± SD spore length for each strain are denoted below. 350 spores per biological replicate (n=3) and strain were measured. Scale bars: 5 μm. **(C)** Yeast two-hybrid analysis to test the interaction between $SepH_{Ms}$ and $FtsZ_{Ms}$ from *M. smegmatis*. Viability of the yeast strains carrying the respective fusion proteins was confirmed by spotting the individual strains on minimal medium lacking leucine and tryptophan (left panel). An interaction between the protein fusions allows growth on minimal medium lacking leucine, tryptophan, histidine and alanine (right panel). Shown is a representative image. Experiments were performed in triplicates. **(D)** Assembly dynamics of $FtsZ_{Ms}$ from *M. smegmatis* using dynamic light scattering. Light scatter traces for 6 μM FtsZ (black) and 6 μM $FtsZ_{Ms}$ in the presence of 3 μM $SepH_{Ms}$ (red) are shown. 2 mM GTP was added to induce FtsZ polymerization. Light scatter graphs display representative traces of at least 3 independent experiments. **(E)** $FtsZ_{Ms}$ filament morphology visualized by negative stain TEM of 6 μM $FtsZ_{Ms}$ alone, with 2mM GTP and with 6 μM $SepH_{Ms}$. $SepH_{Ms}$ (3μM) does not form visible structures when incubated with GTP. Scale bars: 200 nm. **(F)** High and low speed co-sedimentation assay of polymerized $FtsZ_{Ms}$ (6 μM) with and without $SepH_{Ms}$ (3 μM) in the presence of 2 mM GTP. Presence of $FtsZ_{Ms}$ and $SepH_{Ms}$ in the supernatant (S) or pellet (P) was analyzed by SDS-PAGE and Coomassie staining. The average percentage of total FtsZ or SepH in the pellet fraction based on results from two independent experiments is indicated below.

Source Data 1. Alignment of SepH proteins used to construct phylogenetic tree in Figure 7A.
Source Data 2. Phylogenetic tree file with bootstrap values used to generate Figure 7A
Source Data 3. Spore measurement data used in Figure 7B.
Source Data 4. Co-sedimentation data used in Figure 7F.
Figure supplement 1. SepH sequence logo.
Figure supplement 1-source data 1. Alignment used to generate SepH sequence logo.
Figure supplement 2. SDS gel showing purified $SepH_{Ms}$ and $FtsZ_{Ms}$.
Figure supplement 3. Size exclusion chromatogram of purified $SepH_{Ms}$.
Figure supplement 3-source data 2. Size exclusion chromatogram data.
Figure supplement 4. GTP hydrolysis rate of FtsZ with and without $SepH_{Ms}$.
Figure supplement 5. TEM image of polymerized $FtsZ_{Ms}$ with $SepH_{Ms}$ at a 1:1 molar ratio.

181 Figure 8

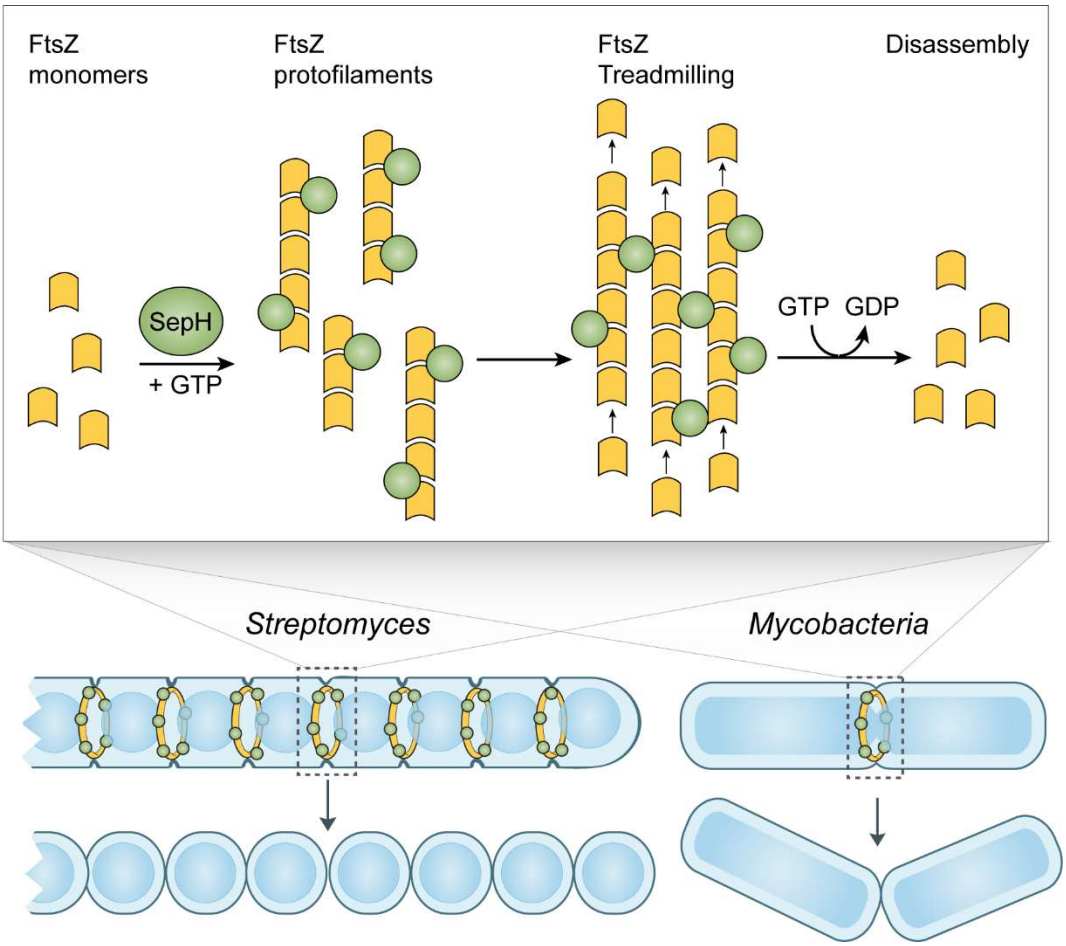

182

183

184 **Figure 8: Model of SepH-mediated FtsZ remodeling in *Streptomyces* and**
185 ***Mycobacterium*.** SepH (green) directly binds FtsZ (yellow) and stimulates the rapid assembly
186 of FtsZ protofilaments. Filament-associated SepH from *M. smegmatis* can further mediate
187 lateral interactions between FtsZ filaments while filaments assembled in the presence of SepH
188 from *S. venezuelae* are less stable. The GTP hydrolysis rate of FtsZ is likely not directly
189 affected by SepH but will eventually lead to the disassembly of FtsZ filaments. Importantly,
190 SepH increases the local concentration of FtsZ which promotes the condensation of filaments
191 into a Z-ring and aids FtsZ treadmilling during the early stages of cell division. This process is
192 linked to septal peptidoglycan synthesis and the formation of division septa.

193

Figure 1-figure supplement 1

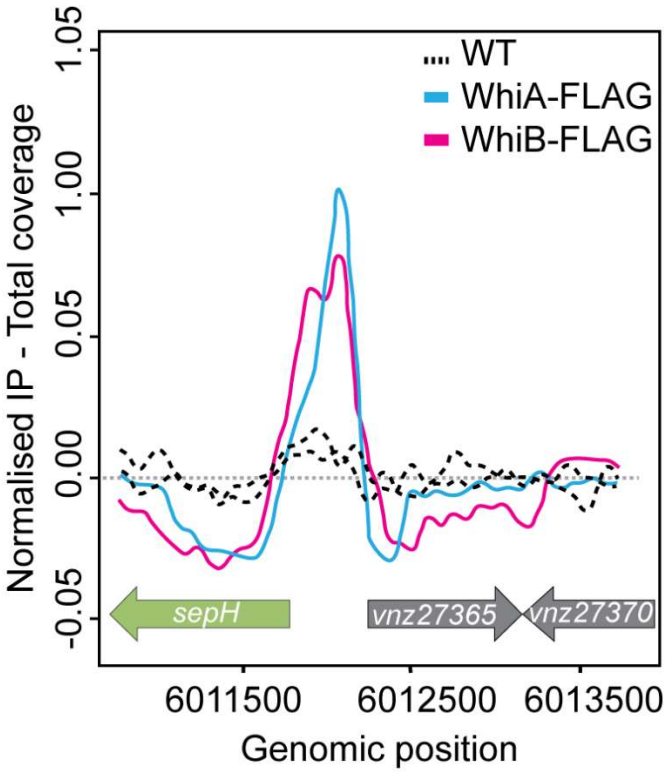

Figure 1-figure supplement 1. Identification of SepH. ChIP-seq traces showing the enrichment of the FLAG-tagged developmental regulators WhiA and WhiB at binding sites upstream of *sepH* or their absence in the untagged wildtype (WT) control sample. Source data: Bush et al. (2013).

Figure 1-figure supplement 2

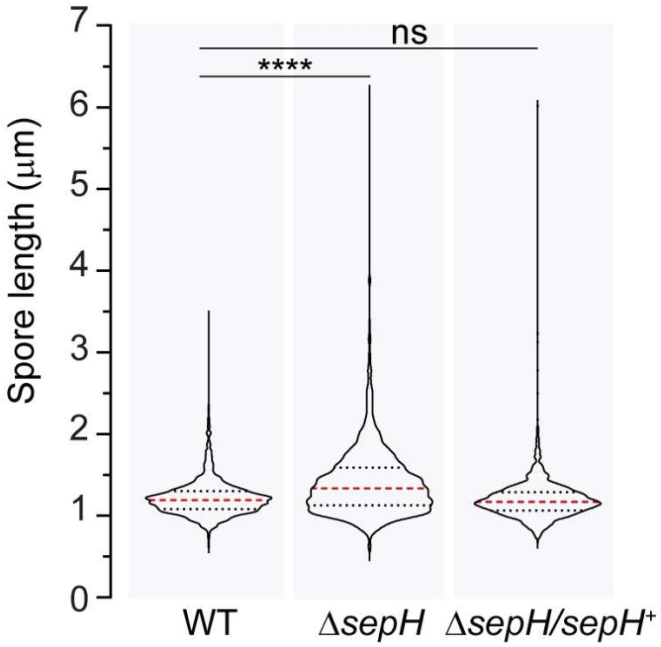

Figure 1-figure supplement 2. Spore length analysis of wildtype *S. venezuelae* (WT), the Δ*sepH* mutant (SV56) and the complemented mutant strain Δ*sepH/sepH*$^{+}$ (MB747). A minimum of 347 spores were quantified for each biological replicate (n=3) and strain. The dashed red lines indicate the median, and black dotted lines the 25/75th percentiles. Statistical comparisons were made using a one-way Anova test followed by a Dunnett's multiple comparison test comparing the means to the WT mean. ****P<0.0001; ns, not significant.

Figure 1-figure supplement 3

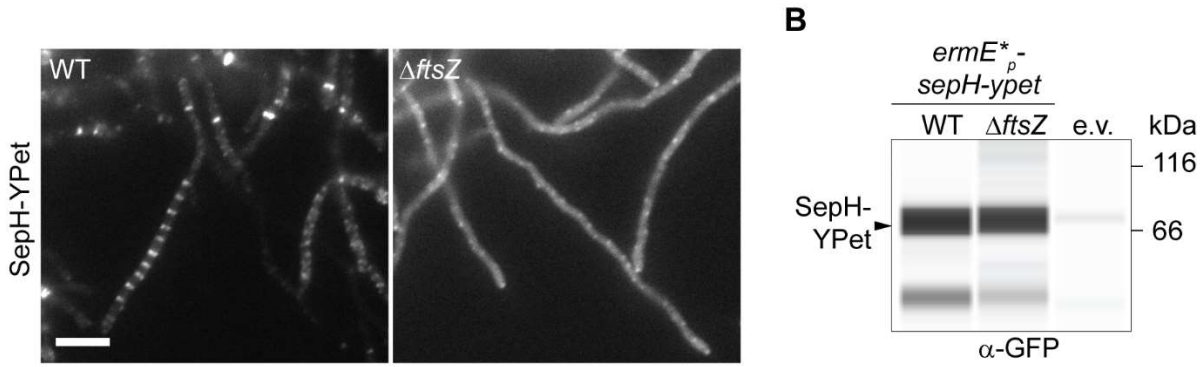

Figure 1-figure supplement 3. Localization and corresponding protein abundance of SepH-YPet in the wildtype and the Δ*ftsZ* mutant. (A) Localization pattern of constitutively produced SepH-YPet in the wildtype (WT, MB858) and in an *ΔftsZ* mutant strain (MB859). Scale bar: 5 μm. **(B)** Automated Western blot showing the accumulation of SepH-YPet in MB858, MB859 and an untagged wildtype control carrying the empty vector (e.v., SS4). YPet fusions were detected with an anti-GFP antibody. Shown are representative results of duplicate experiments.

43 Figure 2-figure supplement 1

44

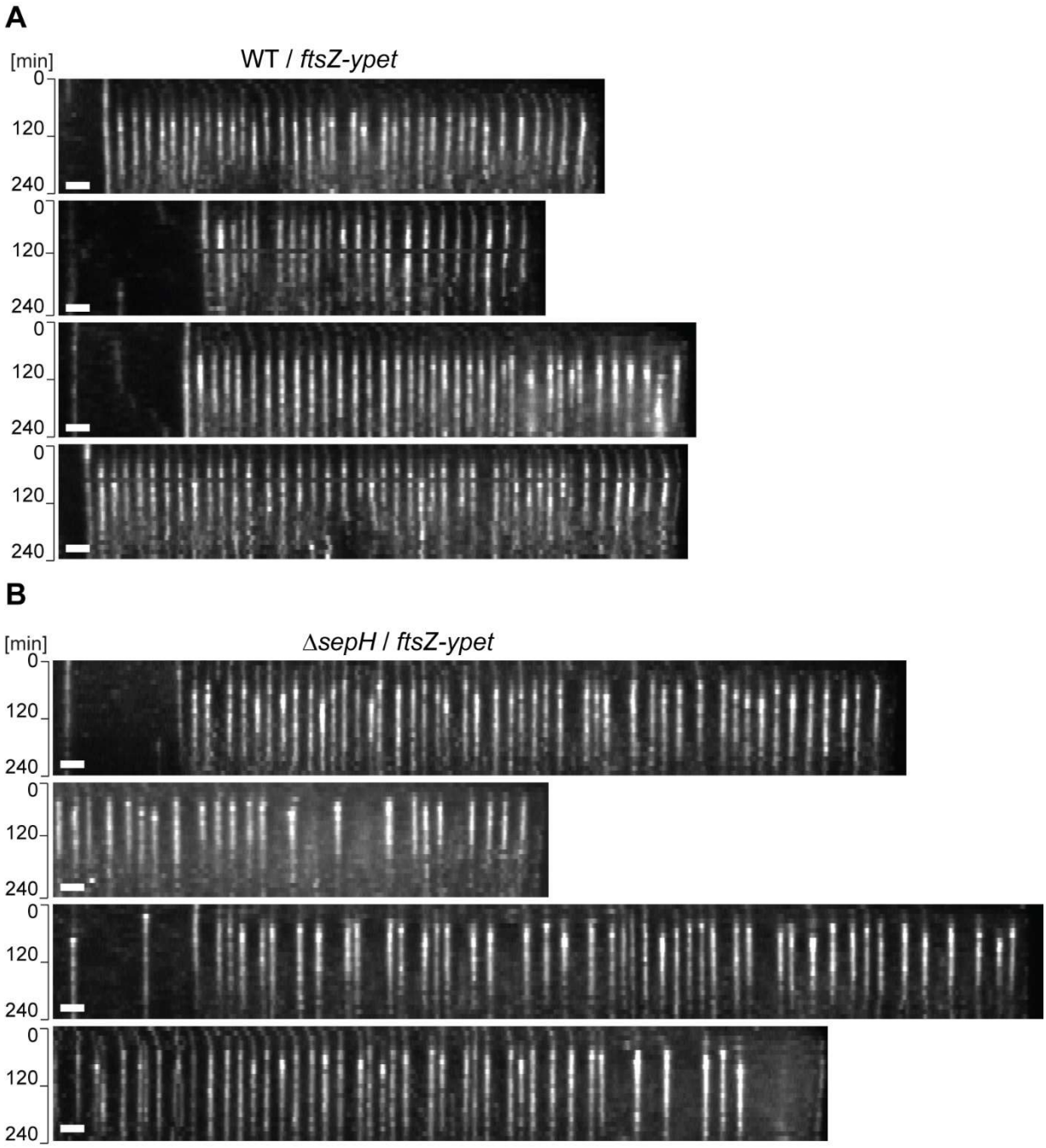

45

46 **Figure 2-figure supplement 1. SepH is important for cell division in *Streptomyces*.**
47 Additional kymographs showing the localization dynamics of FtsZ-YPet in **(A)** wildtype or **(B)**
48 Δ*sepH* cells. Scale bar: 2 μm.

49

Figure 2-figure supplement 2

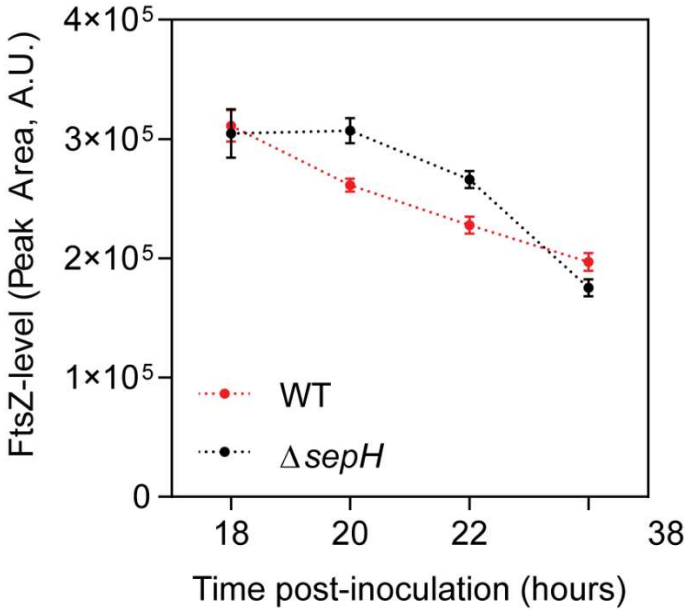

Figure 2-figure supplement 2. FtsZ levels in wildtype and Δ*sepH* cells during sporulation. FtsZ levels were determined by automated Western blot analysis using an anti-FtsZ polyclonal antibody (1:200). Lysates were analyzed in triplicate for each strain and FtsZ levels were quantified at the indicated time-points.

Figure 3-figure supplement 1

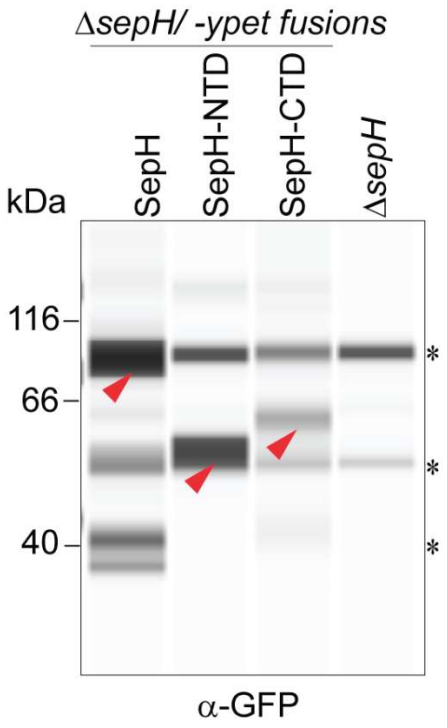

Figure 3-figure supplement 1. Automated Western blot analysis of the different SepH-YPet constructs shown in Figure 3B-D. Strains (MB918, MB827, MB828, SV56) were grown to mid-exponential phase and SepH-YPet fusions were detected using an anti-GFP antibody (1:200). Red arrow heads indicate expected size for each construct. Asterisks denote non-specific signals that are also present in the negative control (Δ*sepH*) or likely degradation products. Shown are representative results of duplicate experiments.

Figure 3-figure supplement 2

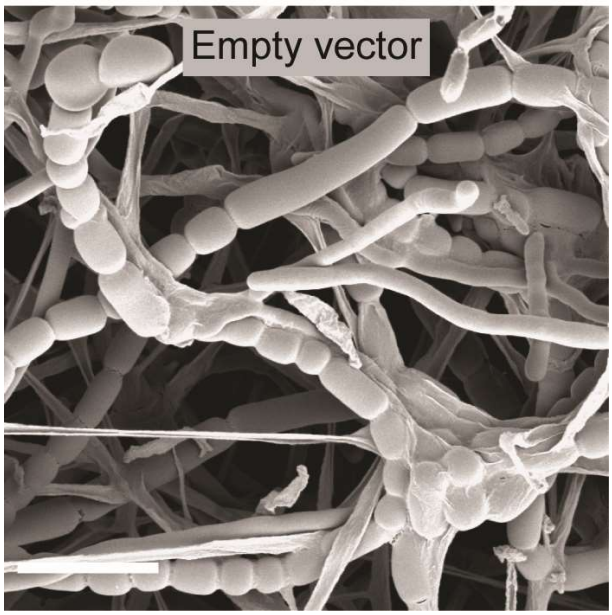

Figure 3-figure supplement 2. Control showing the Δ*sepH* phenotype. Cryo-SEM image showing sporulating hyphae of Δ*sepH* carrying an empty plasmid (MB749). Scale bar: 5 μm.

86 Figure 4-figure supplement 1

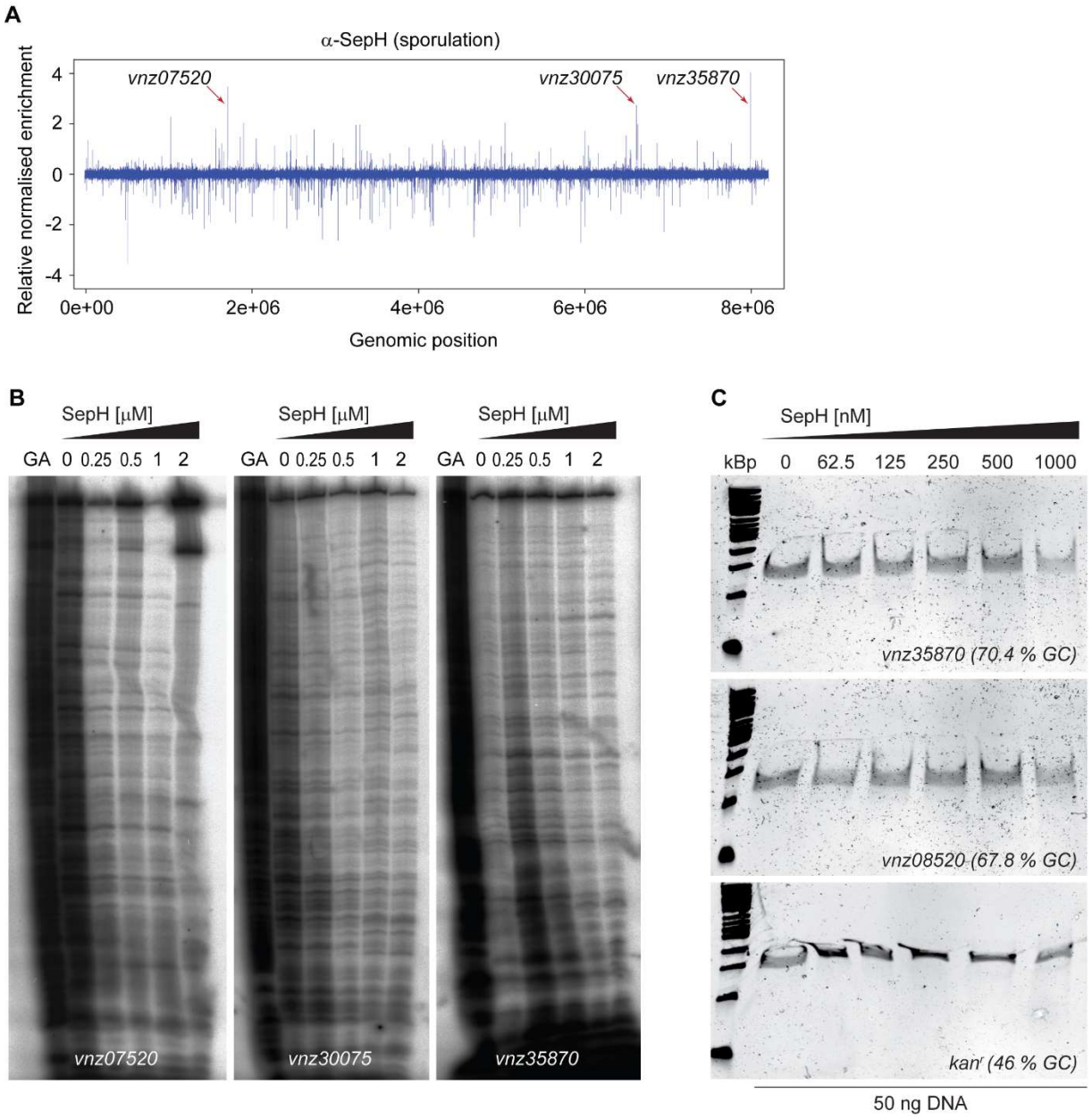

87

88

89 **Figure 4-figure supplement 1. SepH does not bind DNA. (A)** Relative genome-wide
90 distribution of putative SepH binding sites identified by ChIP-seq analysis using an anti-SepH
91 polyclonal antibody during sporulation in wildtype versus Δ*sepH* (SV56) cells. Arrows point to
92 the three most enriched putative binding sites of SepH upstream of *vnz07520*, *vnz30075* and
93 *vnz35870* which were further analyzed in (B) and (C). **(B)** DNase I footprinting analysis of
94 SepH bound to radiolabeled probes derived from the sequence upstream of *vnz07520*,
95 *vnz30075* and *vnz35870*. 5' end-labelled probes were incubated with increasing
96 concentrations of SepH and subjected to DNase I treatment. The footprints are flanked by
97 Maxam and Gilbert sequence ladders (GA). No binding of SepH to the probes could be

98 detected. **(C)** EMSA analysis to test for binding of SepH to the promoter region of *vnz35870*,
99 a sequence internal to *vnz08520* (*ftsZ*) and a low-GC sequence from the Kan^R-gene. No
100 binding activity of SepH to any of the tested DNA probes could be detected.

101

Figure 5-figure supplement 1

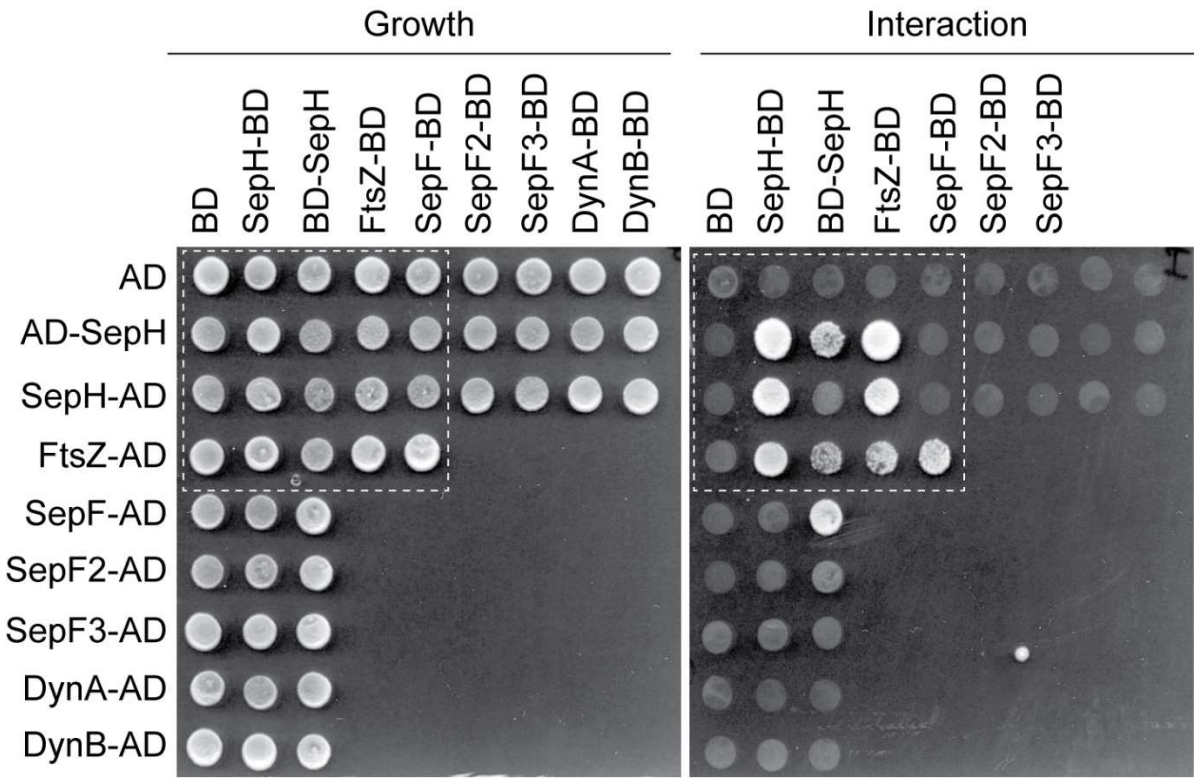

Figure 5-figure supplement 1. Yeast-two hybrid analysis showing the complete set of tested interactions between SepH and different cell division proteins. Growth and putative interaction between the different fusion proteins was verified by spotting the individual strains onto minimal media lacking either leucine and tryptophan (growth) or leucine, tryptophan, histidine and alanine (interaction). The white dashed box indicates the subset of interactions shown in Figure 5A. Each interaction was tested in triplicate and a representative overview of the results is shown.

115 Figure 5-figure supplement 2

116

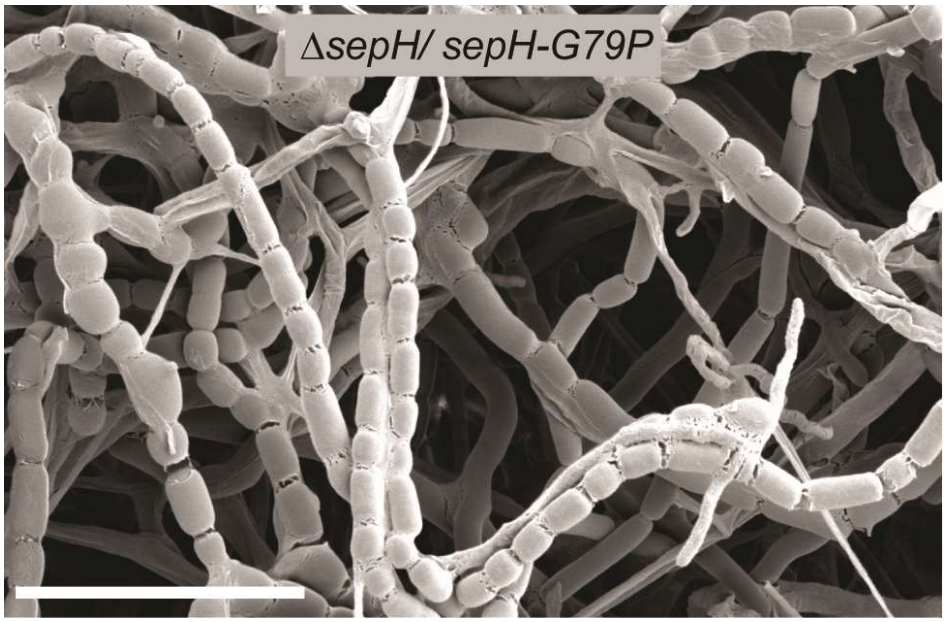

117

118 **Figure 5-figure supplement 2.** Cryo-SEM micrograph of sporulating Δ*sepH* hyphae
119 expressing *sepH-G79P* (MB938). Scale bar: 10 µm.

120

121

122

123

Figure 5-figure supplement 3

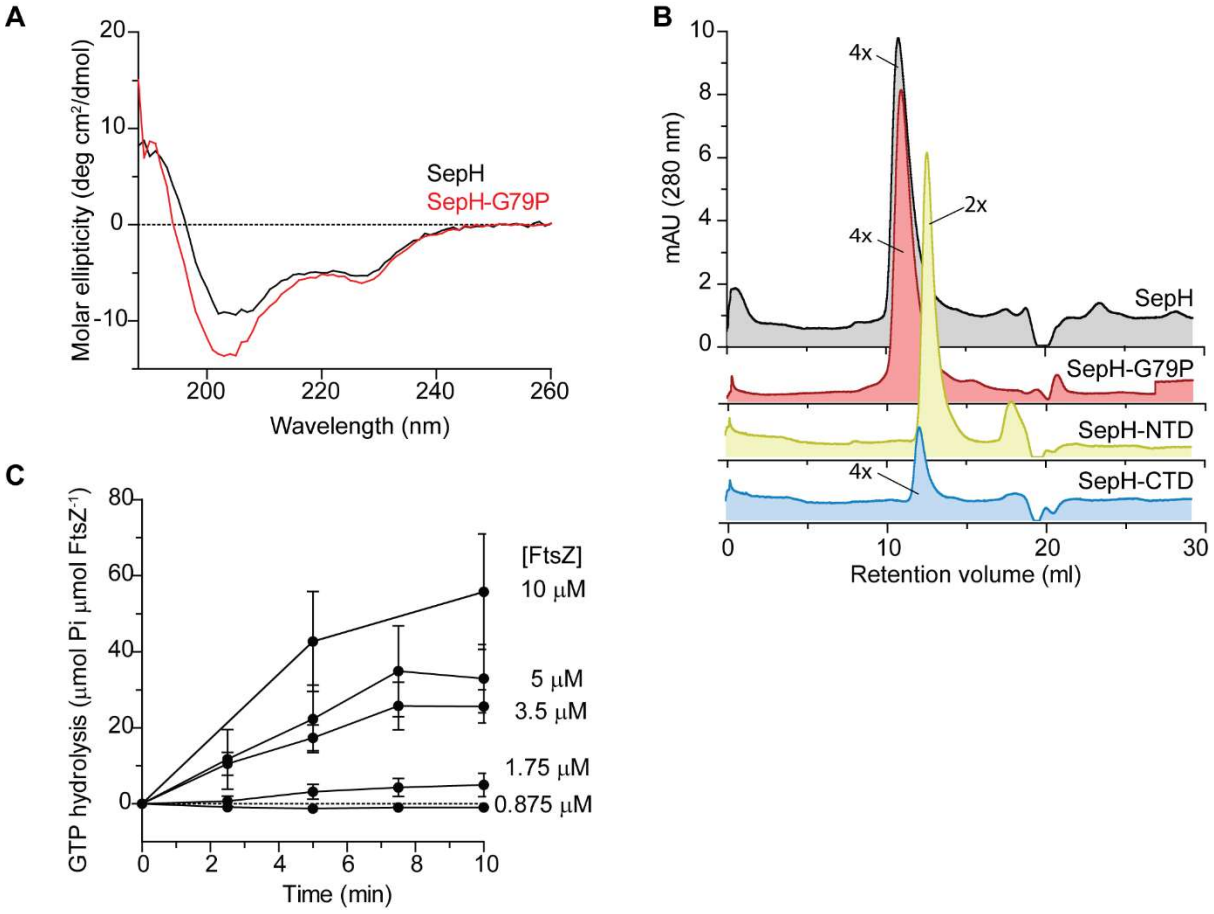

Figure 5-figure supplement 3. Biochemical characterization of SepH, SepH mutant variants and FtsZ. (A) CD spectroscopy analysis of wild-type SepH (black) and SepH-G79P (red). Both proteins show a similar spectral pattern indicating that they are not significantly different in their secondary structure. **(B)** Size exclusion chromatograms of purified SepH (grey), SepH-G79P (red), SepH-NTD (yellow) and SepH-CTD (blue). Predicted multimerization states of the purified proteins based on the migration of MW standards is indicated (4X, tetramer; 2X, dimer). Shown are representative results of duplicate experiments. **(C)** Mean GTP hydrolysis rate of increasing concentrations of FtsZ over time. Error bars represent SEM (n≥3).

Figure 5-figure supplement 4

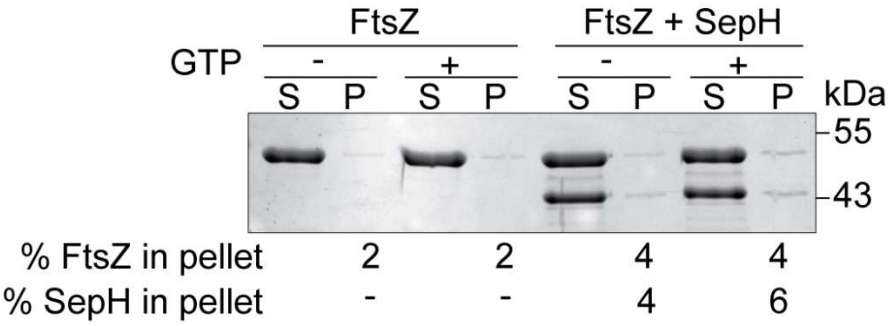

Figure 5-figure supplement 4. Low-speed co-sedimentation. Polymerized FtsZ (3.5 μM) was sedimented in the presence or absence of 3.5 μM SepH and 2 mM GTP. Percentage of total FtsZ or SepH in the pellet fraction averaged from triplicate experiments is indicated below.

145 Figure 6-figure supplement 1

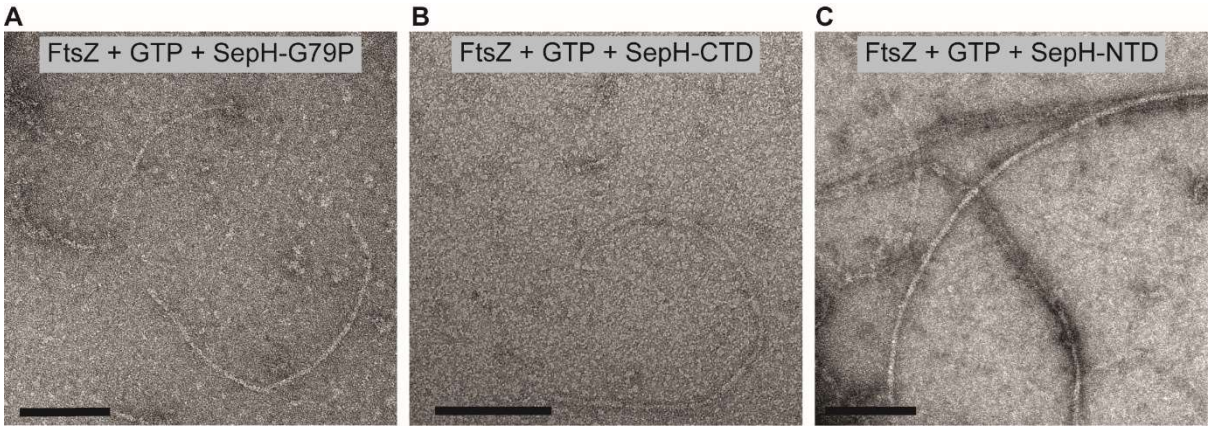

146

147

148 **Figure 6-figure supplement 1. TEM images of polymerized FtsZ with SepH mutant**
149 **variants.** FtsZ was incubated in the presence of GTP and the SepH mutant variants SepH-
150 G79P (A), SepH-CTD (B) or SepH-NTD (C) and filaments were visualized by protein negative
151 stain TEM. Scale bars: 100 nm.

152

153 Figure 6-figure supplement 2

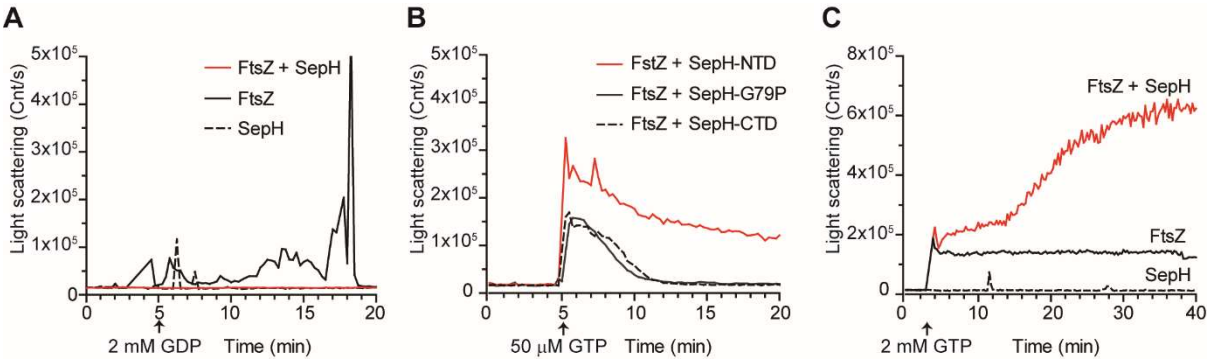

154

155

156 **Figure 6-figure supplement 2. Additional DLS results.** Light scattering traces of 3.5 μM
157 FtsZ assembly kinetics resulting from incubation with **(A)** SepH (3.5 μM) and GDP, **(B)** with
158 50 μM GTP and 3.5 μM of the different SepH mutant variants or **(C)** in the presence of non-
159 limiting GTP concentrations with or without SepH. Light scatter graphs display representative
160 traces of at least 3 independent experiments.

161 Figure 6-figure supplement 3

162

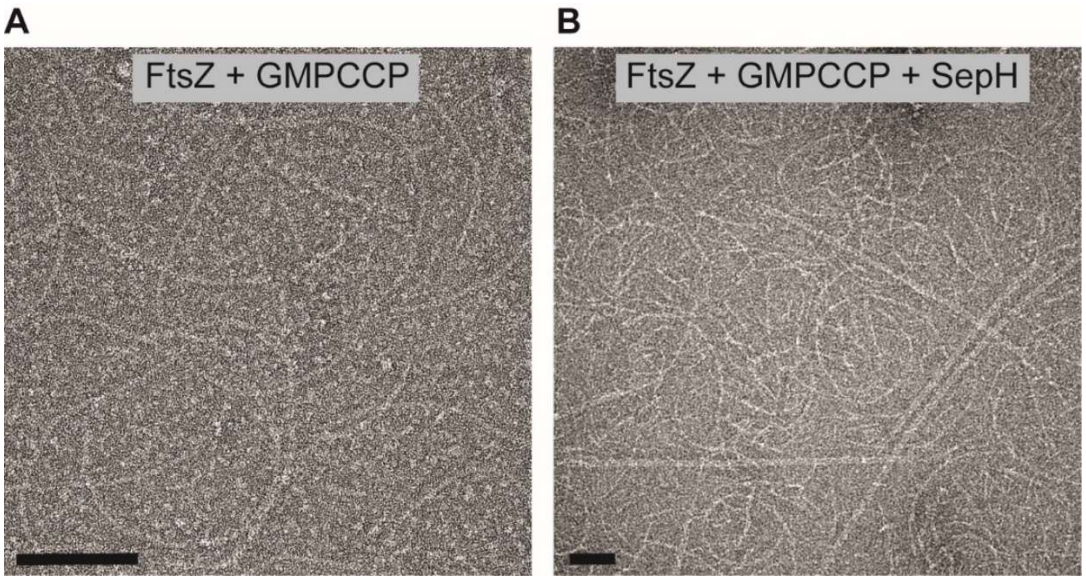

163

164

165 **Figure 6-figure supplement 3: TEM images of FtsZ filaments in the presence of**
166 **GMPCCP and SepH.** FtsZ was incubated with GMPCCP and in the absence (G) or presence
167 of SepH (H) visualized by protein negative stain TEM. Scale bars: 100 nm.

168

169 Figure 7-figure supplement 1

170

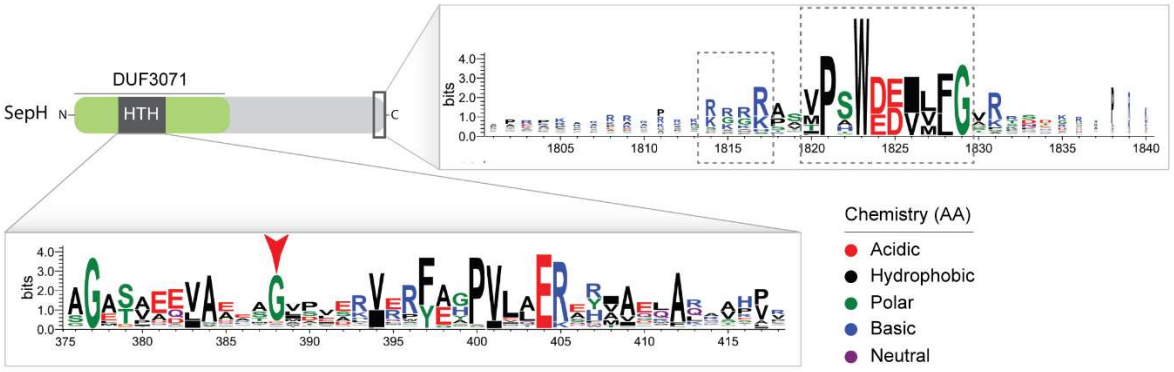

171

172

173 **Figure 7-figure supplement 1. SepH sequence logo.** Logo generated from an alignment of
174 360 selected actinobacterial SepH sequences. Amino acids are colored according to their
175 chemical properties. The SepH N-terminal region contains a highly conserved helix- turn-helix
176 (HTH) motif. The red arrow head denotes glycine residue that was substituted in the *S.*
177 *venezuelae* SepH-G79P variant. The C-terminal domain contains two additional conserved
178 sequence motifs of unknown function (dashed boxes).

179

180 Figure 7-figure supplement 2

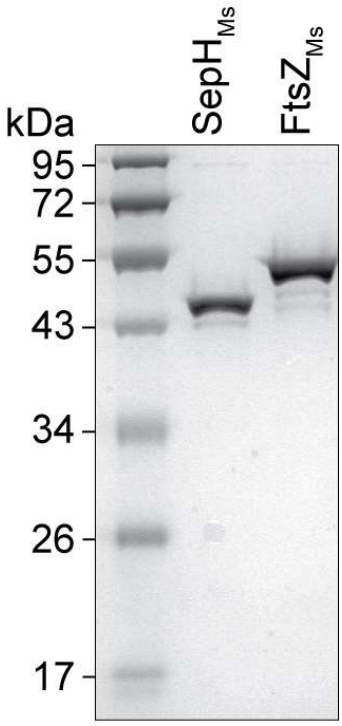

181

182 **Figure 7-figure supplement 2. SDS gel showing purified SepH$_{Ms}$ and FtsZ$_{Ms}$.** Coomassie-
183 stained SDS gel with SepH-6xHis (SepH$_{Ms}$) and untagged FtsZ (FtsZ$_{Ms}$) from *M. smegmatis*.

184

185 Figure 7-figure supplement 3

186

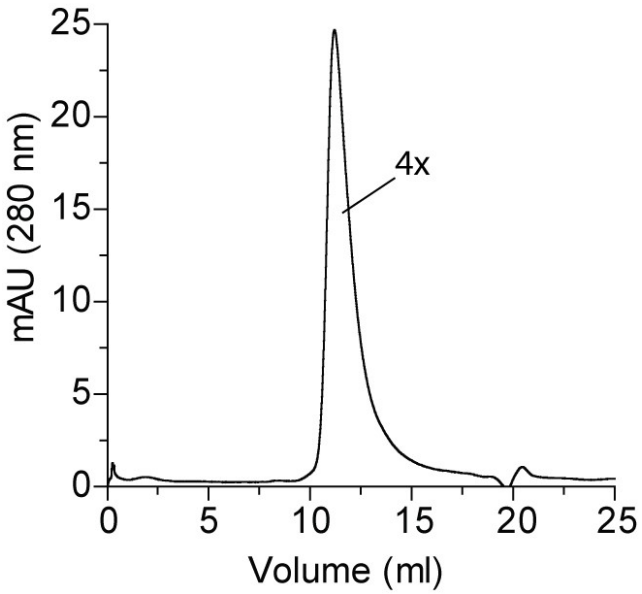

187

188

189 **Figure 7-figure supplement 3. Size exclusion chromatogram**. Shown is the chromatogram
190 of purified $SepH_{Ms}$, which, based on the migration of MW standards, is predicted to form a
191 tetramer (4x). Experiment was performed in duplicate.

192 Figure 7-figure supplement 4

193

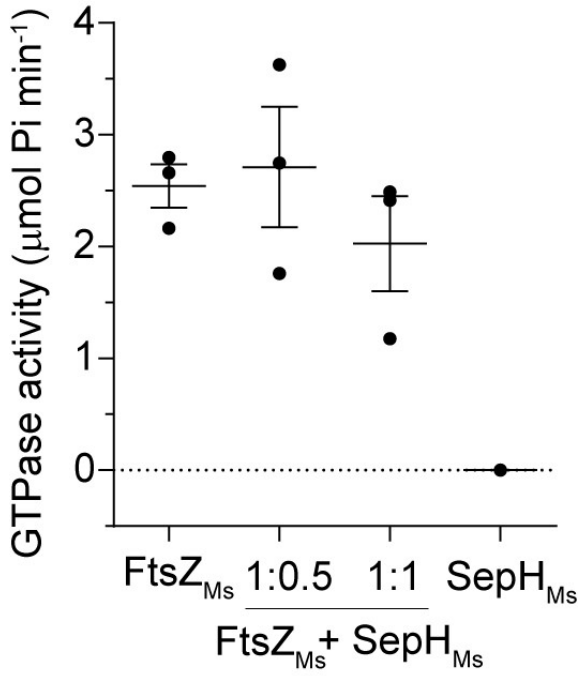

194

195

196 **Figure 7-figure supplement 4. GTP hydrolysis rate of FtsZ with and without $SepH_{Ms}$.**
197 Mean GTP hydrolysis rates of 6 µM $FtsZ_{Ms}$, 3 µM $SepH_{Ms}$ and 6 µM $FtsZ_{Ms}$ in the presence of
198 3 µM $SepH_{Ms}$ (1:0.5) or 6 µM $SepH_{Ms}$ (1:1). Error bars represent SEM (n=3).

199 Figure 7-figure supplement 5

200

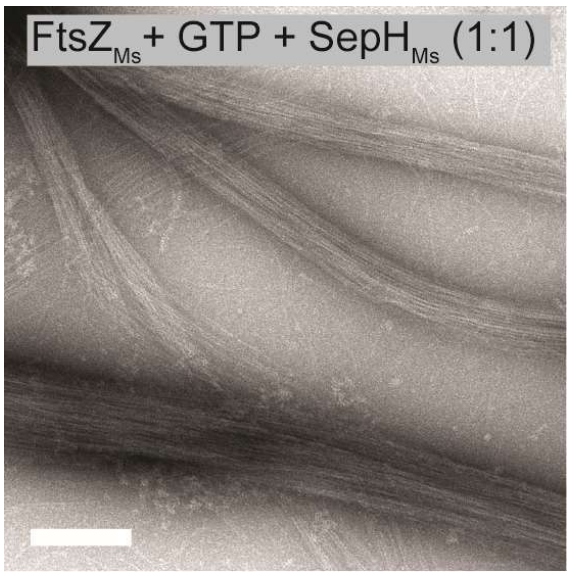

201

202 **Figure 7-figure supplement 5:** $FtsZ_{Ms}$ (6 μM) filament bundles formed in the presence of 6
203 μM $SepH_{Ms}$ and 2mM GTP. Filaments were visualized by negative stain TEM. Scale bar 200
204 nm.

205

Supplementary File legends

Supplementary File 1: Tables listing bacterial strains, plasmids and oligonucleotides used in this study.

Supplementary Movie 1: Time-lapse fluorescence and DIC microscopy movie showing the localization of FtsZ-YPet in growing and sporulating wild-type *S. venezuelae* (SS12). Scale bar: 10 μm.

Supplementary Movie 2: Time-lapse fluorescence and DIC microscopy movie showing growth and localization of FtsZ-YPet in vegetative and sporulating hyphae of the Δ*sepH* mutant (MB750). Scale bar: Scale bar: 10 μm.